

1 **Limited effect of anthropogenic nitrogen oxides on secondary organic**
2 **aerosol formation**

3
4 Yiqi Zheng¹, Nadine Unger^{1, 2}, Alma Hodzic³, Louisa Emmons³, Christoph Knote^{3, 4}
5 Simone Tilmes³, Jean-Francois Lamarque³, and Pengfei Yu^{5, 6}

- 6
7 [1] Department of Geology and Geophysics, Yale University, New Haven, CT, US
8 [2] School of Forestry and Environmental Studies, Yale University, New Haven, CT, US
9 [3] Atmospheric Chemistry Observations and Modeling Laboratory, National Center for
10 Atmospheric Research, Boulder, CO, US
11 [4] Meteorologisches Institut, Ludwig-Maximilians-Universitaet, Munich, Germany
12 [5] Department of Atmospheric and Oceanic Sciences, University of Colorado, Boulder,
13 Colorado, US
14 [6] Laboratory for Atmospheric and Space Physics, University of Colorado, Boulder,
15 Colorado, US

16
17 Correspondence to: Y. Zheng (yiqi.zheng@yale.edu)

1 **Abstract**

2 Globally, secondary organic aerosol (SOA) is mostly formed from emissions of biogenic
3 volatile organic compounds (VOCs) by vegetation, but can be modified by human
4 activities as demonstrated in recent research. Specifically, nitrogen oxides
5 ($\text{NO}_x = \text{NO} + \text{NO}_2$) have been shown to play a critical role in the chemical formation of low
6 volatility compounds. We have updated the SOA scheme in the global NCAR
7 Community Atmospheric Model version 4 with chemistry (CAM4-chem) by
8 implementing a 4-product Volatility Basis Set (VBS) scheme, including NO_x -dependent
9 SOA yields and aging parameterizations. Small differences are found for the no-aging
10 VBS and 2-product schemes; large increases in SOA production and SOA-to-OA ratio
11 are found for the aging scheme. The predicted organic aerosol amounts capture both the
12 magnitude and distribution of US surface annual mean measurements from the
13 Interagency Monitoring of Protected Visual Environments (IMPROVE) network by 50%,
14 and the simulated vertical profiles are within a factor of two compared to Aerosol Mass
15 Spectrometer (AMS) measurements from 13 aircraft-based field campaigns across
16 different region and seasons. We then perform sensitivity experiments to examine how
17 the SOA loading responds to a 50% reduction in anthropogenic nitric oxide (NO)
18 emissions in different regions. We find limited SOA reductions of 0.9 to 5.6%, 6.4 to
19 12.0% and 0.9 to 2.8% for global, the southeast US and the Amazon NO_x perturbations,
20 respectively. The fact that SOA formation is almost unaffected by changes in NO_x can be
21 largely attributed to a limited shift in chemical regime, to buffering in chemical pathways
22 (low- and high- NO_x pathways, O_3 versus NO_3 -initiated oxidation) and to offsetting
23 tendencies in the biogenic versus anthropogenic SOA responses.

1. Introduction

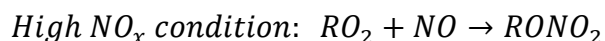
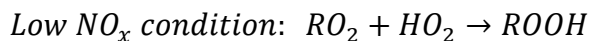
Organic aerosols (OA) account for a substantial fraction of atmospheric fine particulate matter, and can have significant impacts on both air quality (Huang et al., 2014; Zhang et al., 2007) and climate (Carslaw et al., 2010). Previous research suggests that organic compounds make up between 10%~90% of the total aerosol mass at continental mid-latitudes and in tropical forests (Andreae and Crutzen, 1997; Kanakidou et al., 2005; Putaud et al., 2010; Seinfeld and Pankow, 2003). Aside from primary organic aerosols (POA) that are directly emitted into the atmosphere, another major fraction of OA is composed of secondary organic aerosols (SOA), which are formed through chemical transformation of anthropogenic and biogenic volatile organic compounds (AVOCs and BVOCs). AVOCs include aromatics, alkanes and alkenes of about 25, 44 and 38 TgC per year, respectively, from industrial processes, fossil fuel use, biomass burning and road vehicles (Williams and Koppmann, 2007). Isoprene and monoterpenes are the dominant BVOC emissions with estimated global source strengths of about 500 TgC per year and 150 TgC per year, respectively (Guenther et al., 2012). POA can also re-evaporate upon dilution and participate in the chemical oxidation processes leading to the formation of SOA (Robinson et al. 2007).

Biogenic SOA (BSOA) is usually regarded as natural aerosol and as such cannot be addressed by emission control legislation. Recent research implied that anthropogenic compounds facilitate BSOA formation, thus providing the possibility to control BSOA by

1 regulating the emission of other precursor pollutants like AVOCs, POA and nitrogen
2 oxides (Carlton et al., 2010; Emanuelsson et al., 2013; Hoyle et al., 2011; Lin et al., 2013;
3 Rollins et al., 2012; Volkamer et al., 2006). For example, Carlton et al. (2010) have
4 shown that in the southeast US, up to 50% of the total BSOA surface atmospheric loading
5 is attributed to controllable pollution emissions. Spracklen et al. (2011) found that at the
6 global scale the model with a large human-interfered SOA source was the most consistent
7 with observations, which includes a maximum of 10% SOA (10 Tg year^{-1}) from fossil
8 sources, and the extra is mostly likely due to an anthropogenic pollution enhancement of
9 BSOA. The potential impacts of human activities are visible in every step of BSOA
10 formation: the amount of naturally emitted BVOCs through land use and land cover
11 change, the oxidative transformation of BVOCs to semivolatiles through altering
12 atmospheric oxidants concentrations, and the partitioning behavior to the aerosol phase
13 through modifying the load and miscibility of pre-existing organic aerosol (Hoyle et al.,
14 2011).

15
16 Among the multiple human-induced influences, nitrogen oxides ($\text{NO}_x = \text{NO} + \text{NO}_2$, emitted
17 from many fossil-fuel driven activity sectors) play a critical role in SOA formation
18 through several aspects. First, through the competitive chemistry of organo-peroxy
19 radicals (RO_2) formed from oxidation of AVOC and BVOC precursors, which can react
20 mainly with NO at high NO_x or hydroperoxyl (HO_2) and peroxy radicals (RO_2) at low
21 NO_x conditions (Kroll and Seinfeld, 2008; Ziemann and Atkinson, 2012). Calculating the
22 SOA yield dependence on NO_x is challenging because the OH/O_3 ratio depends on the
23 VOC/NO_x ratio (Presto et al., 2005). Lane et al. (2008) suggested that SOA yields could

1 be calculated by a linear combination of the “pure” mass yields scaled by the strength of
2 each branch. In many SOA models (e.g. Heald et al., 2008; Lane et al., 2008; Pye et al.,
3 2010), the representative reactions for each branch are:



4 For AVOCs like light aromatics (Ng et al., 2007) and BVOCs like isoprene (Kroll et al.,
5 2006) and monoterpenes (Presto et al., 2005), both the ROOH groups and the RONO₂
6 groups can be low in volatility thus facilitating SOA formation, but RONO₂ is not the
7 dominant product of the $RO_2 + NO$ channel, therefore the high-NO_x pathway usually has
8 lower yields of SOA. Second, NO_x can influence SOA formation through nighttime
9 nitrate radical (NO₃) chemistry. This pathway has a distinctive chemical signature due to
10 the high yields of organic nitrate (RONO₂), which also forms during daytime
11 photooxidation in the presence of NO but with a lower yield. The importance of NO₃-
12 initiated SOA formation have been confirmed by chamber experiments (Griffin et al.,
13 1999; Ng et al., 2008) and field studies, e.g. in Bakersfield, California, NO₃-chemistry
14 contributed approximately a third of the nighttime increase in total OA (Rollins et al.,
15 2012). Finally, NO_x levels can impact the atmospheric oxidation capacity. In the NO_x-
16 limited regime (in terms of O₃ formation), the OH-initiated oxidation of CO, methane
17 (CH₄) and other VOCs in the presence of NO_x produces O₃. Thus in such conditions,
18 increasing NO_x by human activities should, in principle, lead to the increase in
19 atmospheric oxidation capacity (OH and O₃) (Seinfeld and Pandis, 2006), and result in
20 higher SOA yields. For example, using a chemical transport model PMCAMx, Lane et al.
21 (2008) suggested that a 50% reduction in NO_x emissions could decrease predicted

1 ground-level BSOA by an average of $0.5 \mu\text{g m}^{-3}$ in the eastern US by lessening the
2 atmospheric oxidant levels.

3
4 Due to the multiple impacts of NO_x on SOA formation, it is important to understand how
5 NO_x emission controls alter the particulate matter atmospheric loading. The goal of this
6 study is to improve the SOA scheme in a global climate-chemistry model by
7 incorporating a 4-product Volatility Basis Set (VBS) framework (Pye et al., 2010), which
8 has 4 representative volatility bins to better represent the volatility distribution of all
9 semivolatiles in the atmosphere than the default 2-product scheme (Heald et al., 2008;
10 Odum et al., 1996). The model is then used to investigate the impacts of anthropogenic
11 NO_x emission reduction on SOA formation. Section 2 describes the observational
12 datasets used in this study. In Section 3, we describe the default and updated SOA
13 parameterizations embedded within the global chemistry-climate model framework. We
14 perform control simulations using six different model configurations, including the
15 default 2-product scheme and the updated SOA scheme with and without NO_x -dependent
16 yields for monoterpene, and with and without simplified SOA aging parameterizations.
17 Section 4 shows the results. The control simulations are evaluated and assessed against
18 several observational datasets. Then, we perform sensitivity simulations to probe the
19 impacts of a global 50% anthropogenic NO emission reduction on SOA production. We
20 conduct this experiment as a simplified potential future scenario based on the 50% NO_x
21 emission reduction from power plants in the southeast US by pollution control programs
22 in the past decade (Frost et al., 2006; Kim et al., 2006). Section 5 summarizes the
23 findings of this study.

2 Terminology and Data sets

Table 1 summarizes major abbreviations used in this study. The term OA refers to the total particle phase organic matter including carbon, hydrogen, oxygen and other possible elements. The term OC refers to only the mass of carbon in these organic compounds. Both OA and OC are used based on different measurement techniques. Similarly, primary organic carbon (POC) is the carbon mass in POA; secondary organic carbon (SOC) is the carbon mass in SOA. In this study the term SOA (secondary organic aerosol) and SOG (secondary organic gas) refer to particle phase and gas phase, respectively.

2.1 IMPROVE OC measurements. The US total OC dataset is from the Interagency Monitoring of Protected Visual Environments (IMPROVE, Hand et al., 2011). IMPROVE OC is collected using quartz fiber filters for 24 hours every third day, analyzed offline by thermal optical reflectance (TOR) (Chow et al., 1993), and corrected for an approximate positive artifact (Dillner et al., 2009). Assumptions made in this correction may not always be appropriate (Watson et al., 2009), and the potential negative artifacts due to the volatilization of particulate organics are not accounted. We choose 120 surface sites from IMPROVE network that are within the bottom layer in corresponding model grids. The original 3-day data from 2005 to 2009 has been averaged to seasonal and annual mean values. OC concentrations from sites within the same model grid cell ($1.9^{\circ} \times 2.5^{\circ}$ latitude by longitude) are averaged for comparison to modeled OC concentrations in corresponding model grid cells.

1

2 **2.2 Aircraft-based OA measurements from Aerosol Mass Spectrometer (AMS).** The
3 OA datasets come from 13 aircraft field campaigns that took place between 2005 and
4 2009 (Heald et al., 2011). In these campaigns, total OA density was measured using AMS
5 in standard temperature and pressure conditions (STP: 298K, 1atm), and provides fast on-
6 line submicron aerosol composition (Canagaratna et al., 2007). For each field campaign,
7 the 1-minute raw data is averaged temporally and horizontally along the flight track for
8 comparison to the simulated monthly mean OA vertical profile in corresponding month
9 and location in the model. Each observed OA profile is further averaged vertically to a
10 single value for comparison to the simulated OA concentration averaged over the same
11 range of altitudes.

12

13 **2.3 Surface OA/OOA/HOA measurements from AMS.** We select 42 surface AMS
14 measurements in 2000-2008 from previous studies (Spracklen et al., 2011; Zhang et al.,
15 2007) that differentiate between hydrocarbon-like OA (HOA, a surrogate for POA from
16 combustion and biomass burning) and oxygenated OA (OOA, a surrogate for SOA from
17 all sources). The HOA and OOA are determined by a multiple component analysis
18 (MCA, Zhang et al. 2007). The averaged OOA, HOA and OA data for each campaign
19 have been compared to the simulated monthly mean SOA, POA and total OA in the
20 corresponding model grid. Most of these measurements were taken before 2005. We did
21 not perform simulations in this period due to the lack of GEOS-5 meteorological data
22 (described in Section 3.1). Therefore the model results are averaged from 2005 to 2009 as
23 a climatology to compare with this observational dataset.

3. Modeling framework

3.1 CAM4-chem model. The global Community Atmosphere Model Version 4 with chemistry (CAM4-chem) is part of the Community Earth System Model (CESM, version 1.2.2) (Tilmes et al., 2015). Here, we employ CAM4-chem in its specified dynamics mode, in which CAM and the Community Land Model (CLM) are driven by offline Goddard Earth Observing System Model Version 5 (GEOS-5) reanalysis meteorological fields (available since 2004). The prescribed sea surface temperature and sea ice data are from the Climatological/Slab-Ocean Data Model (DOCN) and Climatological Ice Model (DICE) as other components of CESM. In this configuration, CAM4-chem is run in a Chemistry-Transport Model mode, such that direct comparison can be performed without having to consider variability associated with internally generated meteorology. CAM4-chem includes interactive simulation of O_3 - NO_x -CO-VOC and bulk aerosol chemistry (based on the MOZART-4 chemical mechanism) as described in Lamarque et al., (2012). The default 2-product SOA scheme is described in Sect. 3.2 and in Heald et al. (2008). Updates performed for the purpose of this study are discussed in Section 3.3 and 3.4. The emission of isoprene and monoterpenes are calculated online by Model of Emissions of Gases and Aerosols from Nature (MEGAN-2.1), which is embedded in CLM (Guenther et al., 2012). The anthropogenic, biomass burning and other (except biogenic) emissions in CESM are as described in Lamarque et al. (2012). These consist of anthropogenic emissions from the Precursors of Ozone and their Effects in the Troposphere (POET) inventory for 2000 (Granier et al., 2005), with Asia replaced by Regional Emission

inventory for ASia (REAS-v1) for each year (Ohara et al., 2007). The biomass burning emissions are from GFED-v2 (van der Werf et al., 2006) for 2005-2008 and from the Fire INventory of NCAR (FINN-v1) for 2009 (Wiedinmyer et al., 2010). All the SOA schemes discussed in this study consider that SOA are only generated from oxidization of gas-phase VOCs. The SOA formation from organic compounds emitted originally in the condensed phase is not considered. Simulations are performed with a 30 minute time step, a horizontal resolution of $1.9^{\circ} \times 2.5^{\circ}$ and 56 levels from the surface to approximately 40 km.

3.2 Default SOA parameterization

In CAM4-chem, the default SOA formation follows the 2-product approach (Odum et al., 1996). Each parent VOC is oxidized to generate 2 semivolatile surrogates, which can partition into pre-existing organic particles including both POA and SOA. The partitioning of the semivolatile products is described by absorptive partitioning theory into carbonaceous aerosol material (Donahue et al., 2006; Pankow, 1994). CAM-chem tracks POC in its emission, transport and deposition module. Later in Section 4.2, we assume a POA-to-POC ratio of 1.4 (Aiken et al., 2008; White and Roberts, 1977) to calculate modeling POA and OA to compare with observations. The model simulates anthropogenic SOA (ASOA) from NO_x -dependent OH-initiated oxidation of anthropogenic aromatics (benzene, toluene and xylene), BSOA from the OH-initiated oxidation of isoprene, and the ozonolysis, OH- and NO_3 -initiated oxidation of monoterpene (Table 2). The surrogate SOA products are assumed to be: $\text{C}_{10}\text{H}_{16}\text{O}_4$ for SOA from monoterpene (SOAM), $\text{C}_5\text{H}_{12}\text{O}_4$ for SOA from isoprene (SOAI), $\text{C}_6\text{H}_7\text{O}_3$,

1 $C_7H_9O_3$, and $C_8H_{11}O_3$ for SOA from benzene, toluene and xylenes, therefore the O:C
2 ratio is constant for each SOA species. The overall O:C ratio in total OA depends on the
3 split between POA and SOA, and the fraction of each SOA species. Fossil content is
4 regarded as POA including both hydrophobic and hydrophilic compounds and is not
5 included in SOA in CAM4-chem. The default 2-product model in CAM4-chem only
6 applies low- NO_x yields parameterization for all OH- and O_3 -initiated BSOA formation.
7 The SOA mass yields (summarized in Table S1) are from Heald et al. (2008) and
8 references therein.

10 **3.3 Updated SOA scheme**

11 We update the SOA model to include a 4-product VBS scheme, which has 4 semivolatile
12 surrogates for each parent VOC species. The saturation concentrations (C^*) at 295K for
13 the 4 product groups are 0.1, 1, 10, 100 $\mu g\ m^{-3}$, respectively. This VBS has a wider range
14 of volatilities than the default 2-product parameterization that can better represent the
15 volatility distribution of atmospheric semivolatiles. Another goal of implementing this
16 VBS framework is to facilitate implementation of advanced processing including the
17 aging effect. Changing the enthalpies of vaporization (see Table S1, S2) has no
18 significant effect on simulated SOA burden (difference smaller than 2%). In addition to
19 the current reactions used in the 2-product model, we have added the NO_x -dependent
20 pathway for SOA formation from monoterpenes and the NO_3 -initiated oxidation of
21 isoprene into the VBS (see Table 2). SOA formed from OH-initiated photooxidation of
22 isoprene still only has one set of yields following the low- NO_x parameterizations. We do
23 not change this isoprene-SOA parameterization to remain consistent with the VBS

1 framework from Pye et al. (2010). Additional simulations that include the high-NO_x
 2 pathway of isoprene chemistry are discussed in the Supplement. The SOA mass yields
 3 (summarized in Table S2) are from Pye et al. (2010) and references therein.

4

5 In the 4-product VBS model, the partitioning between the high-NO_x (RO₂+NO) and low-
 6 NO_x (RO₂+HO₂) pathway is determined by the branching ratio β (Pye et al., 2010):

$$\beta = \frac{[NO]}{[NO] + [HO_2]}$$

7 Thus, 100× β % of the parent hydrocarbon channels through the high-NO_x pathway, and
 8 100×(1- β)% of the parent hydrocarbon channels through the low-NO_x pathway. This
 9 format of β is a simplification of:

$$\beta = \frac{\sum k_{RO_2+NO} \times [NO]}{\sum k_{RO_2+NO} \times [NO] + \sum k_{RO_2+HO_2} \times [HO_2]}$$

10 where k_{RO_2+NO} and $k_{RO_2+HO_2}$ represent the reaction rate coefficients of RO₂+NO and
 11 RO₂+HO₂, respectively.

12

13 Field studies that quantified the elemental composition of OA indicate the importance of
 14 aged oxygenated OA (Aiken et al., 2008; Chen et al., 2011; Heald et al., 2010). Several
 15 regional modeling studies have found the “aging” process necessary to produce
 16 reasonable OA mass (Athanasopoulou et al., 2013; Hodzic and Jimenez, 2011; Knote et
 17 al., 2015; Lane et al., 2008; Tsimpidi et al., 2010). In this study we implement a
 18 simplified aging parameterization into the global model to provide a rough assessment of

1 the SOA sensitivity in VBS to the effect of aerosol aging. At every model time step, each
2 gas-phase SOA product except for the lowest volatility product ($C^*=0.1\mu\text{g m}^{-3}$) is
3 assumed to be further oxidized by OH with a reaction rate constant k_{OH} of $4\times 10^{-11}\text{ cm}^3$
4 $\text{molec}^{-1}\text{ s}^{-1}$ (Atkinson and Arey, 2003; Tsimpidi et al., 2010), which reduces its volatility
5 by an order of magnitude. The oxygen-to-carbon ratio (O:C) is assumed to be constant
6 for each surrogate SOA product thus increase in SOA mass due to the addition of oxygen
7 is not considered in the aging process. Considering the complexity of various SOA
8 species and the large uncertainties in aging process, the assumption of fixed O:C ratio for
9 each SOA product surrogate is acceptable for global model parameterizations. The aging
10 rate $k_{\text{OH}}=4\times 10^{-11}\text{ cm}^3\text{ molec}^{-1}\text{ s}^{-1}$ is at the high end of previously suggested parameters
11 (Lane et al., 2008). We do simulations with and without this aging parameterization to
12 quantify the possible range of global SOA strengths, and do additional simulations (see
13 Section 3.4) to examine the effect of different aging parameters.

14
15 Particle-phase SOA as well as gas-phase SOG are removed from the atmosphere by wet
16 and dry deposition. Dry deposition follows a resistance-in-series formulation (Heald et
17 al., 2008; Wesely, 1998). SOA and other soluble aerosols are removed by both in-cloud
18 scavenging and below-cloud washout (Barth et al., 2000; Lamarque et al., 2012).

20 **3.4 Experiment setup**

21 In this study, we apply six different treatments of SOA formation, as summarized in
22 Table 2. ‘2-product’ is the default SOA model; ‘VBS’ and ‘VBS_agHigh’ are the updated
23 4-product VBS scheme with and without the aging effect. ‘VBS_agHigh’ applies the high

aging rate $k_{OH}=4\times 10^{-11}$ cm³ molec⁻¹ s⁻¹ to all species, thus presumably providing the higher bound of simulated SOA loadings. These three schemes (2-product, VBS and VBS_agHigh) are the main SOA schemes that we use to compare with observations (Section 4.2) and study the sensitivity to NO_x perturbations. For each of the three schemes, we perform one control run and one sensitivity run in which anthropogenic NO emissions are reduced by 50% (Section 4.3). We perform additional simulations to explore the impact of different aging and NO_x-dependency parameterizations: ‘VBS_agLow’ applies a lower k_{OH} of 5.2×10^{-12} cm³ molec⁻¹ s⁻¹ (Hu et al., 2013) to all species, which is close to the lower limit suggested by other studies (Hodzic and Jimenez, 2011; Spracklen et al., 2011); ‘VBS_agAVOC’ applies $k_{OH}=4\times 10^{-11}$ cm³ molec⁻¹ s⁻¹ to AVOCs only, as suggested by some studies that ASOA ages longer than does BSOA (Lee-Taylor et al., 2015). ‘VBS_lowNO_x’ is the same as ‘VBS’ except that all SOAM is assumed to be formed through the low-NO_x (RO₂+HO₂) pathway. This ‘VBS_lowNO_x’ scheme is done to isolate the influence of the NO_x-dependent pathway for SOAM formation, which is not considered in the default 2-product settings. All simulations are conducted for the years 2004 to 2009 with offline meteorology from GEOS-5 reanalysis and specific monthly anthropogenic emissions. The year 2004 result is discarded as spin-up.

4. Results

4.1 Comparison of various SOA schemes

1 The annual mean zonally averaged SOA concentration is shown in Fig. 1. The tropical
2 maximum in the lower troposphere is due to large year-round Amazonian BVOC
3 emissions coupled with extensive seasonal biomass burning that provides ample pre-
4 existing POA onto which the semivolatiles can condense. The second surface maximum
5 in the northern hemisphere mid-latitudes 30°-60° is mostly attributed to (1) summertime
6 BVOC emissions from broadleaf deciduous forest in the temperate and boreal zones,
7 especially the southeast US, which has very high BVOC emissions in the summer
8 (Guenther et al., 2006), (2) plentiful supply of anthropogenic and biomass burning
9 emitted POA, and (3) large amounts of AVOC emissions from human activities. In most
10 simulations, indicated by the white contour lines in Fig. 1, the BSOA from isoprene and
11 monoterpenes oxidation accounts for more than 70% of the total SOA in most latitudes
12 and altitudes, which actually includes both ‘naturally-formed’ and ‘anthropogenically-
13 influenced’ BSOA. The rest is ASOA from the oxidation of AVOCs. In the
14 VBS_agAVOC run, ASOA accounts for a larger fraction in Northern Hemisphere mid-
15 latitudes than other simulations ranging from 30% to 50% because in this scheme aging
16 process is only applied to ASOA.

17
18 Table 3 details the annual global SOA budget in each control experiment. Compared to
19 the default 2-product approach, the VBS scheme predicts a smaller global annual burden
20 of SOA (19% lower than the 2-product), although the surface concentration is 11%
21 higher with compensating lower concentrations at higher elevations. Due to the higher
22 yields in the VBS (see Table S1 and S2), more parent hydrocarbon is consumed near the
23 source location and less is transported to upper troposphere relative to the 2-product

1 scheme. Their different volatility also contributes to the difference in SOA
2 concentrations. Table 3 suggests a shorter SOA lifetime of 8.9 days in the VBS than the
3 lifetime of 11.4 days in the 2-product scheme due to the larger wet-deposition flux, which
4 is consistent with the higher surface concentration. The SOA global burden in the
5 VBS_lowNO_x run is 14% higher than the VBS. This is consistent with the fact that the
6 high-NO_x (RO₂+NO) channel is less SOA-producing comparing to the low-NO_x
7 (RO₂+HO₂) channel. The yields of SOAM at 10 µg m⁻³ under high- and low-NO_x are
8 0.09 and 0.19, respectively (Table S2).

9
10 For present climate, the differences in annual burden between the 2 VBS models without
11 aging effect (VBS and VBS_lowNO_x) and the 2-product model are relatively small
12 (<20%), because for most parent hydrocarbon species they are fitted into the same
13 chamber data (see Heald et al. (2008), Pye et al. (2010) and references therein). In
14 contrast, in VBS_agHigh, adding the aging effect accelerates the shift of volatile mass
15 towards lower volatility bins and hence more mass in the particle phase, and results in an
16 overall doubling of the net SOA (particle phase) production, which is important for SOA
17 environmental impacts. We find that the SOA production is sensitive to the assumed OH
18 oxidation rate constant (k_{OH}) for aging of the semivolatile intermediates. For example,
19 using VBS_agLow scheme with a lower k_{OH} of 5.2×10⁻¹² cm³ molec⁻¹ s⁻¹ (Hu et al.,
20 2013), the annual mean SOA production rate would be 44.6±2.0 Tg[C] year⁻¹, in
21 comparison to a production rate of 58.6±2.4 Tg[C] year⁻¹ in the VBS_agHigh scheme
22 with k_{OH} = 4×10⁻¹¹ cm³ molec⁻¹ s⁻¹, and a production rate of 28.6±1.6 Tg[C] year⁻¹ in the
23 VBS scheme without aging parameterization. This single aging parameter represents the

multi-generational aging of hundreds of thousands oxidation intermediate species that are involved in the SOA formation (Lee-Taylor et al., 2015) and is currently not well characterized for individual precursors and chemical environments. In the rest of this study, we will use the three schemes, 2-product, VBS and the VBS_agHigh, to compare with observations and explore the NO_x-dependent effects.

4.2 Evaluation of OA in CAM4-chem simulations

4.2.1 Comparison with the IMPROVE network OC observations

The IMPROVE surface observations and the model outputs are averaged from 2005 to 2009. Modeled OC concentrations are calculated as the sum of primary carbon (directly emitted and transported in the model) and the carbon contained in each SOA species that is calculated assuming the surrogate SOA products described in Section 3.2. Fig. 2(a) and Fig. 3 show the model-IMPROVE comparison of annual mean surface total OC concentrations using the model 2-product, VBS and VBS_agHigh. The total OC in the 2-product and the VBS are similar to each other and are close to the IMPROVE OC magnitude. They capture the observed spatial distribution within 50% ($r^2=0.45$ and 0.47 , respectively). They capture the low OC values in middle and west inland area, and high OC values in the southeast US where considerable BVOC is emitted from forest as well as POC and AVOC emitted from economic sectors. In the northeast US and some coastal polluted regions in California, OC is greatly overestimated by the models. Fig. 2(c) indicates large simulated POC concentration in these regions while IMPROVE total OC (=POC+SOC) is even not as large as the simulated POC concentrations. Therefore the positive bias of the two no-aging simulations in the northeast US is likely due to an

overestimate of POC emissions in the inventory, or due to the assumption that all POA are non-volatile once emitted and stay in the particle phase until deposition. The fact that IMPROVE sites are predominantly located in remote clean regions might also contribute to this discrepancy. In Fig. 2(b) the white contour lines illustrate the annual mean fraction of SOC in total OC. Table 4 summarizes the fractions in each season. In the two no-aging models, annual mean SOC-to-OC ratio ranges from 20% to 30% in the northeast US and 40% to 60% in the southeast US. Even in summer, the ratio does not exceeds 50% in the northeast US and 70% in the southeast US, which is lower than the suggested values from Ahmadov et al. (2012) and Shrivastava et al. (2008). The aging experiment VBS_agHigh increases the SOC-to-OC ratio greatly (68% and 81% in summertime northeast and southeast US) and overestimates OC across the entire US due to large SOA formation from aging, which is consistent with previous studies that the aging coefficient we apply here ($k_{OH} = 4 \times 10^{-11} \text{ cm}^3 \text{ molec}^{-1} \text{ s}^{-1}$) is at the high end of suggested aging rates. The VBS_agHigh scheme slightly improves the replication of spatial distribution of annual mean OC concentrations ($r^2=0.53$ as compared to 0.45 and 0.47 in the 2-product and VBS schemes) but not in summer ($r^2=0.13$, Table 5). Assuming only ASOA ages, the VBS_agAVOC scheme does not improve the simulated spatial distribution ($r^2=0.48$ in annual average and $r^2=0.18$ in summer, Table 5).

4.2.2 Vertical profiles of OA from aircraft-based AMS measurements

To assess the simulated OA vertical profile in these models, we select 13 aircraft campaigns that had available AMS measurements between 2005-2009. The comparison of vertical profiles is shown in Fig. 4. The VBS_agHigh scheme provides a higher OA

1 concentration than the other two no-aging simulations. Overall, the inter-model
2 differences are smaller than the model-observation differences. In biomass burning
3 influenced regions, the observed OA profile is usually associated with large variations at
4 elevated altitude, indicating sporadic fire plumes. For example, for the AMMA campaign
5 (west Africa), the aircraft tracked biomass-burning plumes, thus giving several maxima
6 of observed mean OA at multiple altitudes. In this case, the observed median value at
7 each layer is a more reliable value for evaluation of the simulations (Heald et al., 2011).
8 The simulated OA profiles in these fire-influenced regions are close to the observed
9 median OA profiles and all are within one standard deviation of observations except at
10 site DODO (west Africa). The enhanced observed concentrations in DODO in the upper
11 troposphere indicate strong deep convection. The discrepancies are likely caused by
12 biases in sub-grid meteorology and vertical transport rather than the chemical formation
13 of SOA or POA emissions. Polluted regions have high OA concentrations at the surface.
14 All three of the simulations capture both the vertical distribution characteristics and
15 magnitude of concentration with the largest model-observation difference within $5 \mu\text{g m}^{-3}$.
16 OA in remote sites is close to zero. The models capture OA at IMPEX (west North
17 America and east Pacific) and OP3 (Borneo) sites but overestimate at TROMPEX (Cape
18 Verde) and VOCALS-UK (south Pacific). Generally, the simulated OA profiles are all
19 within a factor of 2 of the observed magnitude, indicating a reasonable model
20 performance across different regions and seasons. Fig. 5 compares OA concentrations
21 averaged across each entire campaign. All the three simulations underestimate observed
22 OA in most campaigns, except in remote sites TROMPEX (Cape Verde) and VOCALS-
23 UK (eastern south Pacific ocean). The VBS_agHigh scheme has the lowest root-mean-

square difference (rmsd) of 1.45, and captures 56% of observed OA mean concentrations, as compared to 50% and 52% in the 2-product and VBS schemes.

4.2.3 OA, SOA and POA from surface AMS measurements

The observed OOA is a surrogate for SOA, and HOA is a surrogate for POA in AMS measurements (Aiken et al., 2009; Lanz et al., 2007; Zhang et al., 2005). We use 42 short-term surface AMS measurements (Spracklen et al., 2011; Zhang et al., 2007) and classify their locations into four groups: North America (17 sites), Europe (12 sites), East Asia (12 sites) and Amazon (1 site). Most of these measurements were taken before 2005. The 2005-2009 monthly mean model results have been averaged into a climatology to compare to the observations, which may lead to large model-observation differences. Fig. 6 compares the measured and simulated OA, OOA(SOA) and HOA(POA). The comparisons between observations and simulations show large discrepancies (in opposite directions) for primary and secondary species. POA is identical in the three simulations. Consistent with the comparison with the IMPROVE network in Section 4.2.1, the models overestimate POA in most regions especially in North America, which will promote condensation of semivolatiles onto pre-existing organic matter thus forming more SOA. The SOA concentration in the two no-aging models, 2-product and VBS, are close to observed OOA in North America and are lower in other regions. By including the aging, the VBS_agHigh simulation increases SOA concentration, leading to an overestimation in North America and still an underestimation in most other regions. The total OA concentrations in all the models exceed observed OA in North America. In Fig. 7 we plot the comparison of SOA(OOA)-to-OA ratios from the observations and simulations. The

2-product and VBS models significantly underestimate the observed OOA-to-OA ratios that range from 0.4 to 1. The VBS_agHigh model makes an improvement but is still lower than the observations due to the large amount of simulated POA. Overall, the inter-model differences are smaller than the model-observation differences. These conclusions are consistent with Section 4.2.1 and 4.2.2.

4.3 The impact of anthropogenic NO_x pollution on surface SOA

For each of the 2-product, VBS and VBS_agHigh schemes, we perform a control run and a sensitivity run in which the anthropogenic NO emissions are reduced by 50% to explore the impact of NO_x pollution on surface SOA concentrations. Other NO sources including biomass burning and soil emissions are not changed. The 50% reduction in anthropogenic NO emissions leads to a 36% decrease in annual mean total NO emissions and a 38% decrease in surface NO_x concentrations at global scale (Fig. S1). The global surface level of oxidants OH, O₃ and NO₃ decrease by 13%, 8% and 29%, respectively (Fig. S2). The surface NO/HO₂ ratio has been greatly reduced by 67%, while the change in branching ratio ($\beta = \frac{NO}{NO+HO_2}$) is small (-3.4%), indicating the NO concentration in the model is too high for HO₂ to compete. The spatial distribution and probability density function of β are plotted in Fig. S3 and Fig. S4. We choose a polluted and a clean region as examples: the southeast US [32°-40°N, 95°-77°W] and the Amazon [17°S-5°N, 77°-55°W], both of which are mostly in the NO_x-limited regime in terms of ozone formation due to their large BVOC emissions (Lane et al., 2008), i.e. the concentration of O₃ and OH are positively related to concentration of NO_x. We examine the dependence of annual mean surface SOA concentrations on β and oxidants level at the global scale, and over the

southeast US and the Amazon regions in Fig. 8. The comparison of the sensitivity (red) and the control runs (green) indicates that the 50% reduction in anthropogenic NO emissions leads to a small decrease in β , oxidation level and SOA concentrations. In Fig. 8, the small SOA concentrations associated with small β values ($\beta < 0.6$) mostly happen over the ocean (not shown) or polar regions where VOC precursors hardly exist and NO_x concentrations are low. In the range $0.6 < \beta < 1.0$, the common regime over land, the highest SOA concentrations occur at relatively lower β values, which mostly locate in tropical rain forests with large BVOC emissions and high SOA production efficiency through the low-NO_x pathway. The influences of β and oxidant level are tightly related because high β indicating high NO_x is usually associated with high concentrations of oxidants. The dependence of SOA on oxidant concentration indicates a maximum at medium oxidant level of approximately 0.8×10^{12} molecules cm⁻³. The low SOA concentrations at high oxidant level mostly occur in polluted regions where SOA production is overwhelmingly dominated by the high-NO_x (low-yields) pathway.

The SOA production in response to NO_x perturbations is complex as described in Section 1. For example, in the VBS_agHigh scheme, we consider monoterpene SOA (SOAM) coming from NO₃-initiated oxidation and the low- and high-NO_x pathway for both OH- and O₃-initiated oxidation. As shown in Fig. 9, with a 50% reduction in anthropogenic NO emissions, total surface SOAM concentration decreases, dominated by the decrease in NO₃-oxidation branch. This decrease in total SOAM mass is a result of addition or cancellation of various changes in each branch, and the relative importance of different branches may alter with different regions. One interesting phenomenon is that when NO_x

emissions are reduced, the low-NO_x OH- and O₃-initiated oxidation branches form less SOAM mass in the Amazon, but more SOAM in human-influenced regions like mid-latitude broadleaf forest in the southeast US, coastal Asia and boreal forest in northern Europe. To further understand and quantitatively evaluate the complex NO_x influence on SOA formation, we examine the predicted change in surface SOA concentrations in different pathways in response to the decrease in anthropogenic NO emissions, as illustrated by Fig. 10. Table 6 details the relative contribution of each pathway to the total SOA change. The results for various SOA types i.e. aromatic SOA, isoprene SOA and monoterpene SOA are discussed below.

4.3.1 Anthropogenic SOAs from benzene, toluene and xylenes: ASOA

ASOA in the three models are assumed to form from OH-initiated oxidation, including both low-NO_x and high-NO_x pathways, i.e. AVOCs+OH(HO₂) and AVOCs+OH(NO). In the southeast US as shown in Fig. 10, all models predict an increase in the low-NO_x pathway and a decrease in the high-NO_x pathway. This is because the model assumes linear interpolation between low- and high-NO_x pathways based on the branching ratio (Section 3.3). When NO_x is reduced, more AVOCs are oxidized under the low-NO_x pathway, which has higher yields (see Table S1 and S2). Due to the limited change in β , the effect of shifting to high-yield HO₂ pathway is very small. The total ASOA formation depends on both the low-/high-pathway partitioning and the oxidation capacity, thus can either increase (e.g. 2-product, VBS) or decrease (VBS_agHigh). In the Amazon, the ASOA changes follow the same pattern as in the southeast US, but their relative contributions are very small due to the low concentrations of AVOCs and anthropogenic

1 NO_x. The contributions of ASOA changes to total SOA change (defined as
2 $\frac{\text{change in ASOA}}{|\text{total SOA change}|}$) ranges from -3.7% to 9.2% in southeast US and from -0.6% to 1.0% in
3 the Amazon.

4

5 **4.3.2 Isoprene SOA: SOAI**

6 In our current models, the isoprene only has one set of yields for OH-initiated daytime
7 oxidation following low-NO_x parameterization, and is oxidized by NO₃ during the night
8 (the latter is not considered in the 2-product model). The OH-oxidation is the dominant
9 branch to form SOAI in both regions. When anthropogenic NO emissions are halved,
10 both OH- and NO₃- initiated branches decrease in the southeast US and the Amazon due
11 to reduced atmospheric OH and NO₃ levels, respectively. The contributions of SOAI
12 changes ($\frac{\text{change in SOAI}}{|\text{total SOA change}|}$) are -46.8% to -73.0% and -30.8% to -43.0% in the two
13 regions.

14

15 **4.3.3 Monoterpene SOA: SOAM**

16 Monoterpenes are oxidized by OH, O₃ and NO₃ in all models but the 2-product model
17 only considers the low-NO_x pathway (Table 2). In the southeast US with large human
18 influence, the surface SOAM formation is largely attributed to NO₃-initiated oxidation as
19 indicated by most models, which dominates the reduction in response to reduced NO_x.

20 This branch itself contributes to the total SOA change ($\frac{\text{change in SOAM from NO}_3\text{-oxidation}}{|\text{total SOA change}|}$)
21 by -48.9% to -65.3%. This reduction in NO₃-branch compared to its normal value is
22 relatively small because the decrease in NO₃ concentration is only 24%. In the VBS and
23 VBS_agHigh models, the partitioning between high- vs. low-NO_x pathway determines

1 the tendency of increasing yielding from the low-NO_x pathway and decreasing yielding
2 through high-NO_x pathway. The OH-oxidation in the southeast US follows such
3 tendency. However, the SOA formed from both high- and low-NO_x pathway of
4 ozonolysis increases. One possible explanation is the “buffering” between O₃- and NO₃-
5 initiated oxidation, both of which mostly happen at night. Compared to the control run,
6 NO₃ is significantly lower in the sensitivity run, thus more monoterpenes would be
7 oxidized by O₃ under both low- and high- NO_x conditions. Adding up the changes in all
8 branches, the SOAM change contributions to total SOA change are about -36.1% to -
9 60.7%. In the Amazon pristine environment, most branches demonstrate a slight
10 reduction in SOAM in all models. Since the absolute magnitude of anthropogenic NO_x is
11 small, the major influence of the NO_x might be the decline in level of atmospheric
12 oxidants: OH, O₃ and NO₃ decrease by 14%, 6% and 16%, respectively. Despite the
13 minor lessening of oxidation capacity, the SOAM reduction and total SOA reduction are
14 negligible.

16 **4.3.4 Summary of surface SOA concentration change**

17 The changes in total SOA concentration at the surface in different regions are
18 summarized in Table 7. In both human-influenced and clean regions, the 50% reduction
19 in anthropogenic NO emissions leads to a decline of BSOA, which dominates the overall
20 SOA decrease. The ASOA could either rise (in models without aging parameterization)
21 or decline (in models with aging considered). Among the multiple effects of NO_x, BSOA
22 is mostly influenced by changes in NO₃-initiated oxidation. Both BSOA and ASOA are

1 also influenced by the change in atmospheric oxidation capacity and the partitioning
2 between high- vs. low-NO_x pathways.

3
4 The annual mean total surface SOA reductions in the southeast US, the Amazon and
5 global average range from 119 to 518, 30 to 153, 3.6 to 43 ng m⁻³, respectively. The
6 corresponding percentage reductions are 6.4 to 12.0%, 0.9 to 2.8% and 0.9 to 5.6%.
7 These changes are comparable with previous estimates (Carlton et al., 2010; Lane et al.,
8 2008), but all are smaller than the magnitude of one standard deviation, indicating that
9 such changes are not statistically significant compared to interannual variations caused by
10 climate and emission variations. The column concentrations of tropospheric SOA are also
11 examined (results not shown here), and the conclusion still holds – no significant change
12 of SOA column concentration when anthropogenic NO emissions are reduced by 50%.
13 One major reason is the small reduction in branching ratio β thus limited shift between
14 high- vs. low-NO_x chemical regimes. The fact that SOA is stable in response to
15 anthropogenic NO_x changes is also attributed to the buffering of various branches (e.g.
16 increased ozonolysis and decreased NO₃-oxidation), the partitioning between low- and
17 high-NO_x pathways and the offset from opposite tendencies of BSOA and ASOA
18 responses (in the no-aging models).

20 **5. Summary**

21
22 NO_x plays a complex role in the chemical formation of SOA. The complexity includes
23 the competition between NO and HO₂ to react with RO₂, its substantial influence on

1 atmospheric oxidation capacity, and the nighttime NO_3 direct oxidation of isoprene and
2 monoterpenes. In this study, we have updated the SOA scheme in the global chemistry-
3 climate model CAM4-chem to include a 4-product VBS scheme that has a broader
4 representation of volatility distribution, and quantitatively evaluated and explained the
5 multiple impacts of anthropogenic NO_x on SOA at global scale.

6
7 We updated the SOA scheme in CAM4-chem to a 4-product VBS scheme. Compared to
8 the default 2-product model, the VBS scheme has 11% higher surface SOA
9 concentration. While the total annual mean SOA burden is 19% smaller (0.69 ± 0.03
10 $\text{Tg}[\text{C}]$ as compared to $0.85 \pm 0.04 \text{ Tg}[\text{C}]$) and lifetime is shorter (8.9 ± 0.2 days as
11 compared to 11.4 ± 0.4 days). Due to the different volatility and higher yields of SOA in
12 the VBS, more VOC is oxidized near surface and less is transported to higher levels, and
13 more SOA is washed out near surface. We explored an aging parameterization with a
14 constant reaction rate with OH ($k_{\text{OH}} = 4 \times 10^{-11} \text{ cm}^3 \text{ molec}^{-1} \text{ s}^{-1}$, the higher-limit in previous
15 studies), which almost doubles the net annual SOA production and significantly increases
16 the SOA concentration both at surface and in the lower free troposphere. The global SOA
17 burden with aging considered (i.e. VBS_agHigh scheme) increases to $1.08 \pm 0.06 \text{ Tg}[\text{C}]$
18 and the corresponding lifetime is 6.7 ± 0.1 days. By applying a lower aging reaction rate
19 ($k_{\text{OH}} = 5.2 \times 10^{-12} \text{ cm}^3 \text{ molec}^{-1} \text{ s}^{-1}$, the lower-limit in previous studies), we found that the
20 simulation of SOA is quite sensitive to the assumed k_{OH} . Despite the significance to SOA
21 formation and properties, the aging effect is still poorly understood at the global scale.
22 Further laboratory and process-modeling constraints at different conditions are needed.

1 The simulated total OC concentrations in the 2-product and the VBS models without
2 aging are similar, and they capture the magnitude and distribution of annual mean surface
3 OC concentrations in the US from the IMPROVE network by 45-47%, but overestimate
4 OC in the polluted northeast US and west coastal regions. The models with an
5 implementation of aging (VBS_agHigh) slightly improve the replication of annual mean
6 spatial distribution ($r^2=53\%$), but overestimate the magnitude. All three models perform
7 poorly in summertime. Compared to AMS measurements from 13 aircraft-based field
8 campaigns, the simulations of OA vertical profiles are within a factor of 2 across
9 different regions and seasons. The VBS_agHigh scheme performs better than the two no-
10 aging models to reproduce these observed OA concentrations ($r^2=56\%$, $\text{rmsd}=1.45$).
11 Further climatological comparisons with surface AMS observations indicate reasonable
12 simulated total OA concentrations but overestimation of POA in some polluted regions,
13 which is consistent with the comparison to the IMPROVE network. This overestimation
14 of POA may come from higher biased POC from emission inventory in certain regions
15 (e.g. the northeast US). If so, it would partially conceal the fact that the current
16 parameterized SOA yields and overlooking of aging in the two no-aging models actually
17 lead to the SOA underestimation. Another possible explanation might be POA re-
18 evaporation and subsequent conversion to SOA (Robinson et al., 2007), indicated by the
19 lower fraction of SOA-to-OA ratio in simulations than the AMS observations. Generally,
20 the inter-model differences are smaller than the model-observation differences. We
21 believe that the updated SOA model (e.g. VBS, VBS_agHigh) is superior to the default
22 one because we implemented the NO_x -dependent SOA formation of monoterpenes,
23 whose absence is a major drawback of the default model. The VBS framework also

1 facilitates inclusion of important processes like aging and the future implementation of
2 size-resolved calculations. The model-observation discrepancies come from several
3 reasons: (1) potential loss of POA due to evaporation and subsequent SOA formation
4 which is currently not considered in this study; (2) uncertainties in chamber-derived SOA
5 yields due to wall losses (Zhang et al., 2014); (3) lack of constraints on dry deposition of
6 organic gases (Hodzic et al., 2014; Knote et al., 2015) or unaccounted photolysis
7 reactions during aging of organics (Hodzic et al., 2015). Other non-chemistry reasons
8 include: (1) the site-level measurement versus coarse model grid ($1.9^{\circ} \times 2.5^{\circ}$); (2) specific
9 observation time period (days to weeks) versus simulated monthly mean values; (3) sub-
10 grid meteorology (e.g. convection events) that the model cannot capture; (4) large
11 uncertainties related to fire activity (e.g. biomass burning plumes).

12
13 Finally, we performed sensitivity experiments to examine how the SOA loading responds
14 to a 50% reduction in anthropogenic NO emissions in different regions. The BSOA
15 generally decreases due to the reduction in NO₃-initiated reaction and the reduced
16 atmospheric oxidation capacity, while the ASOA increases in the two no-aging models
17 mainly because of the increased partitioning to the low NO_x pathway, more AVOCs are
18 oxidized through the low-NO_x pathway that has higher yields. In the aging model, ASOA
19 decreases due to the more important effect of reduced oxidation capacity. Decreases in
20 the total surface SOA concentrations are 6.4 to 12.0%, 0.9 to 2.8% and 0.9 to 5.6% for
21 the southeast US, the Amazon and global NO_x perturbations, respectively, which,
22 however, are not significant. The fact that SOA formation is stable to changes in NO_x can
23 be largely attributed to limited shift in low- and high-NO_x regimes, to buffering in

chemical pathways (e.g. O_3 versus NO_3 -initiated oxidation), and to offsetting tendencies in the biogenic versus anthropogenic SOA responses. Our results, based on the global chemistry-climate model CAM4-chem with simplified SOA schemes, indicate that air quality control on anthropogenic NO_x may not have substantial impacts on organic aerosol loadings at large regional scales. Further modeling studies including both process-based and parameterized schemes need to be done to carefully examine the NO_x impact on SOA formation.

Acknowledgements

Funding support for this study is provided by Yale University, by the National Center for Atmospheric Research, which is operated by the University Corporation for Atmospheric Research on behalf of the National Science Foundation, and by the DOE grant DE-SC0006711 (Alma Hodzic, Christoph Knote). Computing resources are provided by the Climate Simulation Laboratory at NCAR's Computational and Information Systems Laboratory (CISL), sponsored by the National Science Foundation and other agencies.

Disclaimer

Any opinions, findings and conclusions or recommendations expressed in the publication are those of the author(s) and do not necessarily reflect the views of the National Science Foundation.

References:

- Ahmadov, R., McKeen, S. a., Robinson, a. L., Bahreini, R., Middlebrook, a. M., de Gouw, J. a., Meagher, J., Hsie, E.-Y., Edgerton, E., Shaw, S. and Trainer, M.: A volatility basis set model for summertime secondary organic aerosols over the eastern United States in 2006, *J. Geophys. Res.*, 117(D6), 1–19, doi:10.1029/2011JD016831, 2012.
- Aiken, A. C., Decarlo, P. F., Kroll, J. H., Worsnop, D. R., Huffman, J. A., Docherty, K. S., Ulbrich, I. M., Mohr, C., Kimmel, J. R., Sueper, D., Sun, Y., Zhang, Q., Trimborn, A., Northway, M., Ziemann, P. J., Canagaratna, M. R., Onasch, T. B., Alfarra, M. R., Prevot, A. S. H., Dommen, J., Duplissy, J., Metzger, A., Baltensperger, U. and Jimenez, J. L.: O/C and OM/OC ratios of primary, secondary, and ambient organic aerosols with high-resolution time-of-flight aerosol mass spectrometry, *Environ. Sci. Technol.*, 42(12), 4478–4485, doi:10.1021/es703009q, 2008.
- Aiken, A. C., Salcedo, D., Cubison, M. J., Huffman, J. a, Decarlo, P. F., Ulbrich, I. M. and Docherty, K. S.: Mexico City aerosol analysis during MILAGRO using high resolution aerosol mass spectrometry at the urban supersite (T0) – Part 1 : Fine particle composition and organic source apportionment, *Atmos. Chem. Phys.*, 9, 6633–6653, doi:10.5194/acpd-9-8377-2009, 2009.
- Andreae, M. O. and Crutzen, P. J.: Atmospheric Aerosols: Biogeochemical Sources and Role in Atmospheric Chemistry, *Science* (80-), 276(5315), 1052–1058, doi:10.1126/science.276.5315.1052, 1997.
- Athanasopoulou, E., Vogel, H., Vogel, B., Tsimpidi, A. P., Pandis, S. N., Knote, C. and Fountoukis, C.: Modeling the meteorological and chemical effects of secondary organic aerosols during an EUCAARI campaign, *Atmos. Chem. Phys.*, 13(2), 625–645, doi:10.5194/acp-13-625-2013, 2013.
- Barth, M. C., Rasch, P. J., Kiehl, J. T., Benkovitz, C. M. and Schwartz, S. E.: Sulfur chemistry in the National Center for Atmospheric Research Community Climate Model: Description, evaluation, features, and sensitivity to aqueous chemistry, *J. Geophys. Res.*, 105(D1), 1387, doi:10.1029/1999JD900773, 2000.
- Canagaratna, M. R., Jayne, J. T., Jimenez, J. L., Allan, J. D., Alfarra, M. R., Zhang, Q., Onasch, T. B., Drewnick, F., Coe, H., Middlebrook, A., Delia, A., Williams, L. R., Trimborn, A. M., Northway, M. J., DeCarlo, P. F., Kolb, C. E., Davidovits, P. and Worsnop, D. R.: Chemical and microphysical characterization of ambient aerosols with the aerodyne aerosol mass spectrometer, *Mass Spectrom. Rev.*, 26(2), 185–222, doi:10.1002/mas.20115, 2007.
- Carlton, A. G., Pinder, R. W., Bhawe, P. V. and Pouliot, G. a.: To what extent can

1 biogenic SOA be controlled?, *Environ. Sci. Technol.*, 44(9), 3376–3380,
2 doi:10.1021/es903506b, 2010.

3 Carslaw, K. S., Boucher, O., Spracklen, D. V., Mann, G. W., Rae, J. G. L., Woodward, S.
4 and Kulmala, M.: A review of natural aerosol interactions and feedbacks within the Earth
5 system, *Atmos. Chem. Phys.*, 10, 1701–1737, doi:10.5194/acp-10-1701-2010, 2010.

6 Chen, Q., Liu, Y., Donahue, N. M., Shilling, J. E. and Martin, S. T.: Particle-phase
7 chemistry of secondary organic material: Modeled compared to measured O:C and H:C
8 Elemental ratios provide constraints, *Environ. Sci. Technol.*, 45, 4763–4770,
9 doi:10.1021/es104398s, 2011.

10 Chow, J. C., Watson, J. G., Pritchett, L. C., Pierson, W. R., Frazier, C. a. and Purcell, R.
11 G.: The dri thermal/optical reflectance carbon analysis system: description, evaluation
12 and applications in U.S. Air quality studies, *Atmos. Environ. Part A. Gen. Top.*, 27(8),
13 1185–1201, doi:10.1016/0960-1686(93)90245-T, 1993.

14 Dillner, A. M., Phuah, C. H. and Turner, J. R.: Effects of post-sampling conditions on
15 ambient carbon aerosol filter measurements, *Atmos. Environ.*, 43(37), 5937–5943,
16 doi:10.1016/j.atmosenv.2009.08.009, 2009.

17 Donahue, N. M., Robinson, a. L., Stanier, C. O. and Pandis, S. N.: Coupled partitioning,
18 dilution, and chemical aging of semivolatile organics, *Environ. Sci. Technol.*, 40(8),
19 2635–2643, doi:10.1021/es052297c, 2006.

20 Emanuelsson, E. U., Hallquist, M., Kristensen, K., Glasius, M., Bohn, B., Fuchs, H.,
21 Kammer, B., Kiendler-Scharr, a., Nehr, S., Rubach, F., Tillmann, R., Wahner, a., Wu,
22 H.-C. and Mentel, T. F.: Formation of anthropogenic secondary organic aerosol (SOA)
23 and its influence on biogenic SOA properties, *Atmos. Chem. Phys. Discuss.*, 12, 20311–
24 20350, doi:10.5194/acpd-12-20311-2012, 2012.

25 Frost, G. J., McKeen, S. A., Trainer, M., Ryerson, T. B., Neuman, J. A., Roberts, J. M.,
26 Swanson, A., Holloway, J. S., Sueper, D. T., Fortin, T., Parrish, D. D., Fehsenfeld, F. C.,
27 Flocke, F., Peckham, S. E., Grell, G. A., Kowal, D., Cartwright, J., Auerbach, N. and
28 Habermann, T.: Effects of changing power plant NO_x emissions on ozone in the eastern
29 United States: Proof of concept, *J. Geophys. Res.*, 111(D12),
30 doi:D12306r10.1029/2005jd006354, 2006.

31 Granier, C., Guenther, A., Lamarque, J. F., Mieville, A., Muller, J., Oliver, J., Orlando, J.,
32 Peters, J., Petron, G., Tyndall, G. K. and Wallens, S.: POET, a database of surface
33 emissions of ozone precursors, [online] Available from:
34 <http://www.aero.jussieu.fr/projet/ACCENT/POET.php>, 2005.

35 Griffin, R. J., Cocker, D. R., Seinfeld, J. H. and Dabdub, D.: Estimate of global

1 atmospheric organic aerosol from oxidation of biogenic hydrocarbons, *Geophys. Res.*
2 *Lett.*, 26(17), 2721, doi:10.1029/1999GL900476, 1999.

3 Guenther, A. B., Jiang, X., Heald, C. L., Sakulyanontvittaya, T., Duhl, T., Emmons, L. K.
4 and Wang, X.: The model of emissions of gases and aerosols from nature version 2.1
5 (MEGAN2.1): An extended and updated framework for modeling biogenic emissions,
6 *Geosci. Model Dev.*, 5, 1471–1492, doi:10.5194/gmd-5-1471-2012, 2012.

7 Hand, J. L., Copeland, S. a., Day, D. E., Dillner, a. M., Indresand, H., Malm, W. C.,
8 McDade, C. E., Moore, C. T., Pitchford, M. L., Schichtel, B. a. and Watson, J. G.: Spatial
9 and Seasonal Patterns and Temporal Variability of Haze and its Constituents in the
10 United States Report V, , (June 2011), doi:ISSN 0737-5352-87, 2011.

11 Heald, C. L., Coe, H., Jimenez, J. L., Weber, R. J., Bahreini, R., Middlebrook, a. M.,
12 Russell, L. M., Jolleys, M., Fu, T. M., Allan, J. D., Bower, K. N., Capes, G., Crosier, J.,
13 Morgan, W. T., Robinson, N. H., Williams, P. I., Cubison, M. J., Decarlo, P. F. and
14 Dunlea, E. J.: Exploring the vertical profile of atmospheric organic aerosol: Comparing
15 17 aircraft field campaigns with a global model, *Atmos. Chem. Phys.*, 11, 12676–12696,
16 doi:10.5194/acp-11-12673-2011, 2011.

17 Heald, C. L., Henze, D. K., Horowitz, L. W., Feddema, J., Lamarque, J. F., Guenther, a.,
18 Hess, P. G., Vitt, F., Seinfeld, J. H., Godstein, a. H. and Fung, I.: Predicted change in
19 global secondary organic aerosol concentrations in response to future climate, emissions,
20 and land use change, *J. Geophys. Res. Atmos.*, 113, 1–16, doi:10.1029/2007JD009092,
21 2008.

22 Heald, C. L., Kroll, J. H., Jimenez, J. L., Docherty, K. S., Decarlo, P. F., Aiken, a. C.,
23 Chen, Q., Martin, S. T., Farmer, D. K. and Artaxo, P.: A simplified description of the
24 evolution of organic aerosol composition in the atmosphere, *Geophys. Res. Lett.*, 37,
25 doi:10.1029/2010GL042737, 2010.

26 Hodzic, a. and Jimenez, J. L.: Modeling anthropogenically controlled secondary organic
27 aerosols in a megacity: A simplified framework for global and climate models, *Geosci.*
28 *Model Dev.*, 4, 901–917, doi:10.5194/gmd-4-901-2011, 2011.

29 Hodzic, a., Madronich, S., Kasibhatla, P. S., Tyndall, G., Aumont, B., Jimenez, J. L.,
30 Lee-Taylor, J. and Orlando, J.: Organic photolysis reactions in tropospheric aerosols:
31 effect on secondary organic aerosol formation and lifetime, *Atmos. Chem. Phys.*
32 *Discuss.*, 15(6), 8113–8149, doi:10.5194/acpd-15-8113-2015, 2015.

33 Hoyle, C. R., Boy, M., Donahue, N. M., Fry, J. L., Glasius, M., Guenther, a., Hallar, a.
34 G., Huff Hartz, K., Petters, M. D., Petäjä, T., Rosenoern, T. and Sullivan, a. P.: A review
35 of the anthropogenic influence on biogenic secondary organic aerosol, *Atmos. Chem.*

1 Phys., 11, 321–343, doi:10.5194/acp-11-321-2011, 2011.

2 Hu, W. W., Hu, M., Yuan, B., Jimenez, J. L., Tang, Q., Peng, J. F., Hu, W., Shao, M.,
3 Wang, M., Zeng, L. M., Wu, Y. S., Gong, Z. H., Huang, X. F. and He, L. Y.: Insights on
4 organic aerosol aging and the influence of coal combustion at a regional receptor site of
5 central eastern China, *Atmos. Chem. Phys.*, 13, 10095–10112, doi:10.5194/acp-13-
6 10095-2013, 2013.

7 Huang, R.-J., Zhang, Y., Bozzetti, C., Ho, K.-F., Cao, J.-J., Han, Y., Daellenbach, K. R.,
8 Slowik, J. G., Platt, S. M., Canonaco, F., Zotter, P., Wolf, R., Pieber, S. M., Bruns, E. a.,
9 Crippa, M., Ciarelli, G., Piazzalunga, A., Schwikowski, M., Abbaszade, G., Schnelle-
10 Kreis, J., Zimmermann, R., An, Z., Szidat, S., Baltensperger, U., Haddad, I. El and
11 Prévôt, A. S. H.: High secondary aerosol contribution to particulate pollution during haze
12 events in China, *Nature*, doi:10.1038/nature13774, 2014.

13 Kanakidou, M., Seinfeld, J. H., Pandis, S. N., Barnes, I., Dentener, F. J., Facchini, M. C.,
14 Van Dingenen, R., Ervens, B., Nenes, a., Nielsen, C. J., Swietlicki, E., Putaud, J. P.,
15 Balkanski, Y., Fuzzi, S., Horth, J., Moortgat, G. K., Winterhalter, R., Myhre, C. E. L.,
16 Tsigaridis, K., Vignati, E., Stephanou, E. G. and Wilson, J.: Organic aerosol and global
17 climate modelling: a review, *Atmos. Chem. Phys.*, 5, 1053–1123, doi:10.5194/acp-5-
18 1053-2005, 2005.

19 Kim, S. W., Heckel, A., McKeen, S. A., Frost, G. J., Hsie, E. Y., Trainer, M. K., Richter,
20 A., Burrows, J. P., Peckham, S. E. and Grell, G. A.: Satellite-observed U.S. power plant
21 NO_x emission reductions and their impact on air quality, *Geophys. Res. Lett.*,
22 33(L22812), 1–5, doi:10.1029/2006GL027749, 2006.

23 Knote, C., Hodzic, A. and Jimenez, J. L.: The effect of dry and wet deposition of
24 condensable vapors on secondary organic aerosols concentrations over the continental
25 US, *Atmos. Chem. Phys. Discuss.*, 14(9), 13731–13767, doi:10.5194/acpd-14-13731-
26 2014, 2015.

27 Kroll, J. H., Ng, N. L., Murphy, S. M., Flagan, R. C. and Seinfeld, J. H.: Secondary
28 organic aerosol formation from isoprene photooxidation, *Environ. Sci. Technol.*, 40(3),
29 1869–1877, doi:10.1021/es0524301, 2006.

30 Kroll, J. H. and Seinfeld, J. H.: Chemistry of secondary organic aerosol: Formation and
31 evolution of low-volatility organics in the atmosphere, *Atmos. Environ.*, 42, 3593–3624,
32 doi:10.1016/j.atmosenv.2008.01.003, 2008.

33 Lamarque, J. F., Emmons, L. K., Hess, P. G., Kinnison, D. E., Tilmes, S., Vitt, F., Heald,
34 C. L., Holland, E. a., Lauritzen, P. H., Neu, J., Orlando, J. J., Rasch, P. J. and Tyndall, G.
35 K.: CAM-chem: Description and evaluation of interactive atmospheric chemistry in the

- 1 Community Earth System Model, *Geosci. Model Dev.*, 5(3), 369–411, doi:10.5194/gmd-
2 5-369-2012, 2012.
- 3 Lane, T. E., Donahue, N. M. and Pandis, S. N.: Simulating secondary organic aerosol
4 formation using the volatility basis-set approach in a chemical transport model, *Atmos.*
5 *Environ.*, 42, 7439–7451, doi:10.1016/j.atmosenv.2008.06.026, 2008.
- 6 Lanz, V. a., Alfarra, M. R., Baltensperger, U., Buchmann, B., Hueglin, C. and Prévôt, a.
7 S. H.: Source apportionment of submicron organic aerosols at an urban site by factor
8 analytical modelling of aerosol mass spectra, *Atmos. Chem. Phys.*, 7(6), 1503–1522,
9 doi:10.5194/acp-7-1503-2007, 2007.
- 10 Lee-Taylor, J., Hodzic, A., Madronich, S., Aumont, B., Camredon, M. and Valorso, R.:
11 Multiday production of condensing organic aerosol mass in urban and forest outflow,
12 *Atmos. Chem. Phys.*, 14, 595–615, doi:10.5194/acp-15-595-2015, 2015.
- 13 Lin, Y. H., Knipping, E. M., Edgerton, E. S., Shaw, S. L. and Surratt, J. D.: Investigating
14 the influences of SO₂ and NH₃ levels on isoprene-derived secondary organic aerosol
15 formation using conditional sampling approaches, *Atmos. Chem. Phys.*, 13, 8457–8470,
16 doi:10.5194/acp-13-8457-2013, 2013.
- 17 Ng, N. L., Kroll, J. H., Chan, a W. H., Chhabra, P. S., Flagan, R. C. and Seinfeld, J. H.:
18 Secondary organic aerosol formation from m-xylene, toluene, and benzene, *Atmos.*
19 *Chem. Phys.*, 7(3), 3909–3922, doi:10.5194/acp-7-3909-2007, 2007.
- 20 Ng, N. L., Kwan, a J., Surratt, J. D., Chan, a W. H., Chhabra, P. S., Sorooshian, a.,
21 Pye, H. O. T., Crounse, J. D., Wennberg, P. O., Flagan, R. C. and Seinfeld, J. H.:
22 Secondary organic aerosol (SOA) formation from reaction of isoprene with nitrate
23 radicals (NO₃), *Atmos. Chem. Phys. Discuss.*, 8(3), 3163–3226, doi:10.5194/acpd-8-
24 3163-2008, 2008.
- 25 Odum, J. R., Hoffmann, T., Bowman, F., Collins, D., Flagan Richard, C. and Seinfeld
26 John, H.: Gas particle partitioning and secondary organic aerosol yields, *Environ. Sci.*
27 *Technol.*, 30(8), 2580–2585, doi:10.1021/es950943+, 1996.
- 28 Ohara, T., Akimoto, H., Kurokawa, J., Horii, N., Yamaji, K., Yan, X. and Hayasaka, T.:
29 An Asian emission inventory of anthropogenic emission sources for the period
30 1980–2020, *Atmos. Chem. Phys. Discuss.*, 7(3), 6843–6902, doi:10.5194/acpd-7-
31 6843-2007, 2007.
- 32 Pankow, J. F.: An Absorption-Model of the Gas Aerosol Partitioning Involved in the
33 Formation of Secondary Organic Aerosol, *Atmos. Environ.*, 28(2), 189–193,
34 doi:10.1016/j.atmosenv.2007.10.060, 1994.
- 35 Presto, A. a., Huff Hartz, K. E. and Donahue, N. M.: Secondary organic aerosol

1 production from terpene ozonolysis. 2. Effect of NO_x concentration, *Environ. Sci.*
2 *Technol.*, 39(18), 7046–7054, doi:10.1021/es050400s, 2005.

3 Putaud, J. P., Van Dingenen, R., Alastuey, A., Bauer, H., Birmili, W., Cyrys, J., Flentje,
4 H., Fuzzi, S., Gehrig, R., Hansson, H. C., Harrison, R. M., Herrmann, H., Hitzenberger,
5 R., Hüglin, C., Jones, A. M., Kasper-Giebl, A., Kiss, G., Kousa, A., Kuhlbusch, T. A. J.,
6 Löschau, G., Maenhaut, W., Molnar, A., Moreno, T., Pekkanen, J., Perrino, C., Pitz, M.,
7 Puxbaum, H., Querol, X., Rodriguez, S., Salma, I., Schwarz, J., Smolik, J., Schneider, J.,
8 Spindler, G., ten Brink, H., Tursic, J., Viana, M., Wiedensohler, A. and Raes, F.: A
9 European aerosol phenomenology - 3: Physical and chemical characteristics of particulate
10 matter from 60 rural, urban, and kerbside sites across Europe, *Atmos. Environ.*, 44(10),
11 1308–1320, doi:10.1016/j.atmosenv.2009.12.011, 2010.

12 Pye, H. O. T., Chan, a. W. H., Barkley, M. P. and Seinfeld, J. H.: Global modeling of
13 organic aerosol: The importance of reactive nitrogen (NO_x and NO₃), *Atmos. Chem.*
14 *Phys.*, 10, 11261–11276, doi:10.5194/acp-10-11261-2010, 2010.

15 Robinson, A. L., Donahue, N. M., Shrivastava, M. K., Weitkamp, E. a, Sage, A. M.,
16 Grieshop, A. P., Lane, T. E., Pierce, J. R. and Pandis, S. N.: Rethinking Organic
17 Aerosols: Semivolatile Emissions and Photochemical Aging, *Science* (80-.),
18 315(March), 1259–1262, doi:10.1126/science.1133061, 2007.

19 Rollins, a W., Browne, E. C., Pusede, S. E., Wooldridge, P. J., Gentner, D. R., Goldstein,
20 a H., Liu, S., Day, D. a and Cohen, R. C.: Evidence for NO_x Control over Nighttime
21 SOA formation, , 267(September), 1210–1212, 2012.

22 Seinfeld, J. H. and Pandis, S. N.: *Atmospheric Chemistry and Physics: From Air*
23 *Pollution to Climate Change*, 2nd ed., Wiley, New York, USA., 2006.

24 Seinfeld, J. H. and Pankow, J. F.: Organic atmospheric particulate material., *Annu. Rev.*
25 *Phys. Chem.*, 54, 121–140, doi:10.1146/annurev.physchem.54.011002.103756, 2003.

26 Shrivastava, M. K., Lane, T. E., Donahue, N. M., Pandis, S. N. and Robinson, A. L.:
27 Effects of gas particle partitioning and aging of primary emissions on urban and regional
28 organic aerosol concentrations, *J. Geophys. Res. Atmos.*, 113(18), 1–16,
29 doi:10.1029/2007JD009735, 2008.

30 Spracklen, D. V., Jimenez, J. L., Carslaw, K. S., Worsnop, D. R., Evans, M. J., Mann, G.
31 W., Zhang, Q., Canagaratna, M. R., Allan, J., Coe, H., McFiggans, G., Rap, a. and
32 Forster, P.: Aerosol mass spectrometer constraint on the global secondary organic aerosol
33 budget, *Atmos. Chem. Phys.*, 11, 12109–12136, doi:10.5194/acp-11-12109-2011, 2011.

34 Tilmes, S., Lamarque, J.-F., Emmons, L. K., Kinnison, D. E., Ma, P.-L., Liu, X., Ghan,
35 S., Bardeen, C., Arnold, S., Deeter, M., Vitt, F., Ryerson, T., Elkins, J. W., Moore, F. and

1 Spackman, R.: Description and evaluation of tropospheric chemistry and aerosols in the
2 Community Earth System Model (CESM1.2), *Geosci. Model Dev. Discuss.*, 7, 8875–
3 8940, doi:10.5194/gmdd-7-8875-2014, 2014.

4 Tsimpidi, a. P., Karydis, V. a., Zavala, M., Lei, W., Molina, L., Ulbrich, I. M., Jimenez,
5 J. L. and Pandis, S. N.: Evaluation of the volatility basis-set approach for the simulation
6 of organic aerosol formation in the Mexico City metropolitan area, *Atmos. Chem. Phys.*
7 *Discuss.*, 9, 13693–13737, doi:10.5194/acpd-9-13693-2009, 2010.

8 Volkamer, R., Jimenez, J. L., San Martini, F., Dzepina, K., Zhang, Q., Salcedo, D.,
9 Molina, L. T., Worsnop, D. R. and Molina, M. J.: Secondary organic aerosol formation
10 from anthropogenic air pollution: Rapid and higher than expected, *Geophys. Res. Lett.*,
11 33(17), doi:10.1029/2006GL026899, 2006.

12 Watson, J. G., Chow, J. C., Chen, L. W. A. and Frank, N. H.: Methods to assess
13 carbonaceous aerosol sampling artifacts for IMPROVE and other long-term networks., *J.*
14 *Air Waste Manag. Assoc.*, 59(8), 898–911, doi:10.3155/1047-3289.59.8.898, 2009.

15 van der Werf, G. R., Randerson, J. T., Giglio, L., Collatz, G. J., Kasibhatla, P. S. and
16 Arellano, A. F.: Interannual variability of global biomass burning emissions from 1997 to
17 2004, *Atmos. Chem. Phys. Discuss.*, 6(2), 3175–3226, doi:10.5194/acpd-6-3175-2006,
18 2006.

19 Wesely, M. L.: Parameterization of surface resistances to gaseous dry deposition in
20 regional-scale numerical models, *Atmos. Environ.*, 41(SUPPL.), 52–63,
21 doi:10.1016/j.atmosenv.2007.10.058, 1998.

22 White, W. H. and Roberts, P. T.: On the Nature and Origins of Visibility-Reducing
23 Aerosols in the Los Angeles Air Basin, *Atmos. Environ.*, 11, 803–812, 1977.

24 Wiedinmyer, C., Akagi, S. K., Yokelson, R. J., Emmons, L. K., Al-Saadi, J. A., Orlando,
25 J. J. and Soja, A. J.: The Fire INventory from NCAR (FINN) – a high resolution global
26 model to estimate the emissions from open burning, *Geosci. Model Dev. Discuss.*, 3(4),
27 2439–2476, doi:10.5194/gmdd-3-2439-2010, 2010.

28 Zhang, Q., Jimenez, J. L., Canagaratna, M. R., Allan, J. D., Coe, H., Ulbrich, I., Alfarra,
29 M. R., Takami, A., Middlebrook, A. M., Sun, Y. L., Dzepina, K., Dunlea, E., Docherty,
30 K., DeCarlo, P. F., Salcedo, D., Onasch, T., Jayne, J. T., Miyoshi, T., Shimono, A.,
31 Hatakeyama, S., Takegawa, N., Kondo, Y., Schneider, J., Drewnick, F., Borrmann, S.,
32 Weimer, S., Demerjian, K., Williams, P., Bower, K., Bahreini, R., Cottrell, L., Griffin, R.
33 J., Rautiainen, J., Sun, J. Y., Zhang, Y. M. and Worsnop, D. R.: Ubiquity and dominance
34 of oxygenated species in organic aerosols in anthropogenically-influenced Northern
35 Hemisphere midlatitudes, *Geophys. Res. Lett.*, 34, doi:10.1029/2007GL029979, 2007.

- 1 Zhang, Q., Worsnop, D. R., Canagaratna, M. R. and Jimenez, J.-L.: Hydrocarbon-like
2 and oxygenated organic aerosols in Pittsburgh: insights into sources and processes of
3 organic aerosols, *Atmos. Chem. Phys.*, 5(5), 3289–2211, doi:10.5194/acp-5-3289-2005,
4 2005.
- 5 Zhang, X., Cappa, C. D., Jathar, S. H., McVay, R. C., Ensberg, J. J., Kleeman, M. J. and
6 Seinfeld, J. H.: Influence of vapor wall loss in laboratory chambers on yields of
7 secondary organic aerosol., *Proc. Natl. Acad. Sci. U. S. A.*, 111(16), 5802–7,
8 doi:10.1073/pnas.1404727111, 2014.
- 9 Ziemann, P. J. and Atkinson, R.: Kinetics, products, and mechanisms of secondary
10 organic aerosol formation, *Chem. Soc. Rev.*, 41(19), 6582, doi:10.1039/c2cs35122f,
11 2012.

12

1 **Table 1. Abbreviations used in this study.**

Abbreviations	Description
OA	Organic aerosol, including the mass of carbon, oxygen and other possible elements. $OA = POA + SOA$
OC	Organic carbon. $OC = POC + SOC$
POA	Primary organic aerosol.
POC	Primary organic carbon.
SOA	Secondary organic aerosol.
SOC	Secondary organic carbon.
SOG	Secondary organic gas.
ASOA	Anthropogenic secondary organic aerosol.
BSOA	Biogenic secondary organic aerosol.
AVOC	Anthropogenic volatile organic compounds.
BVOC	Biogenic volatile organic compounds.
SOAM	SOA from monoterpene oxidation.
SOAI	SOA from isoprene oxidation.
MTP	Monoterpenes.
ISOP	Isoprene.
HOA	Hydrocarbon-like organic aerosol, a surrogate for POA.
OOA	Oxygenated organic aerosol, a surrogate for SOA.

2

3

4

1

2 **Table 2. Summary of SOA treatments in CAM4-chem model runs.**

SOA scheme	Reactions to form SOA	Description
2-product	MTP+OH(HO ₂); MTP+O ₃ (HO ₂); MTP+NO ₃ ; ISOP+OH(HO ₂); AVOCs+OH(HO ₂); AVOCs+OH(NO).	Default 2-product scheme; SOA mass yields summarized in Table S1 (Heald et al., 2008).
VBS	MTP+OH(HO ₂); MTP+O ₃ (HO ₂); MTP+OH(NO); MTP+O ₃ (NO); MTP+NO ₃ ; ISOP+OH(HO ₂); ISOP+NO ₃ ; AVOCs+OH(HO ₂); AVOCs+OH(NO).	Updated 4-product VBS scheme; SOA mass yields summarized in Table S2 (Pye et al., 2010)
VBS_lowNO _x	MTP+OH(HO ₂); MTP+O ₃ (HO ₂); MTP+NO ₃ ; ISOP+OH(HO ₂); ISOP+NO ₃ ; AVOCs+OH(HO ₂); AVOCs+OH(NO).	Same as VBS, but assuming all monoterpene SOA (SOAM) is formed under low-NO _x conditions
VBS_agHigh	Same as VBS	Same as VBS, with multi-generational aging applied to all species; $k_{OH}=4\times 10^{-11} \text{ cm}^3 \text{ molec}^{-1} \text{ s}^{-1}$.
VBS_agLow	Same as VBS	Same as VBS, with multi-generational aging applied to all species; $k_{OH}=5.2\times 10^{-12} \text{ cm}^3 \text{ molec}^{-1} \text{ s}^{-1}$.
VBS_agAVOC	Same as VBS	Same as VBS, with multi-generational

		aging applied to ASOA only; $k_{\text{OH}}=4\times 10^{-11} \text{ cm}^3 \text{ molec}^{-1} \text{ s}^{-1}$.
--	--	--

1

1 Table 3. Summary of simulated annual mean global budget of SOA (particle-phase).

	Burden Tg[C]	Net SOA production Tg[C] year⁻¹	Lifetime Day	Wet deposition Tg[C] year⁻¹	Other losses (by SOA dry deposition) Tg[C] year⁻¹
2-product	0.85±0.04	27.3±2.1	11.4±0.4	-24.4±1.8	-2.9±0.3
VBS	0.69±0.03	28.6±1.6	8.9±0.2	-25.3±1.4	-3.3±0.3
VBS_lowNO_x	0.79±0.03	33.7±1.8	8.5±0.2	-29.8±1.5	-3.9±0.3
VBS_agHigh	1.08±0.06	58.6±2.4	6.7±0.1	-52.1±2.1	-6.5±0.4
VBS_agLow	0.96±0.05	44.6±2.0	7.8±0.1	-40.0±1.7	-4.8±0.3
VBS_agAVOC	0.75±0.03	31.5±1.6	8.6±0.2	-27.8±1.4	-3.7±0.3

2

1 **Table 4. Fraction of SOC in total OC (%) in the southeast US and the northeast US.**

		Annual	MAM	JJA	SON	DJF
Northeast US	2-product	24%	15%	45%	20%	6%
	VBS	28%	19%	49%	23%	8%
	VBS_agHigh	45%	33%	68%	39%	12%
Southeast US	2-product	39%	29%	62%	32%	8%
	VBS	44%	34%	67%	37%	10%
	VBS_agHigh	63%	55%	81%	56%	18%

2

- 1 **Table 5. Coefficients of determination (r^2) of IMPROVE measurements versus**
- 2 **simulated total OC.**

	Annual	MAM	JJA	SON	DJF
2-product	0.45	0.40	0.18	0.41	0.42
VBS	0.47	0.42	0.18	0.43	0.42
VBS_agHigh	0.53	0.54	0.13	0.49	0.45
VBS_agAVOC	0.48	0.45	0.18	0.44	0.44

3

- 1 **Table 6. The relative contributions (%) of each SOA formation pathway to the total**
2 **SOA concentration change in the southeast US and the Amazon, defined as**
3 $\frac{\text{SOA change in each pathway}}{|\text{total SOA change}|}$. The sums of all numbers in each simulation equal -100%
4 because the total SOA change in the sensitivity runs compared to the control runs are
5 always negative. The reaction denotations are the same as defined in Figure 10.

		M1	M2	M3	M4	M5	I1	I2	A1	A2
SE US	2-product	-10.4		+15.0		-65.3	-46.8		+10.6	-3.1
	VBS	+2.9	-13.5	+29.5	+8.8	-63.8	-40.3	-32.7	+13.7	-4.5
	VBS_agHigh	+1.0	-5.3	+8.9	+2.0	-48.9	-35.1	-18.9	+3.5	-7.2
Amazon	2-product	-5.1		-0.2		-65.0	-30.8		+1.4	-0.4
	VBS	+0.4	-7.8	+5.9	-15.8	-45.1	-16.2	-21.9	+0.9	-0.5
	VBS_agHigh	-1.4	-4.3	-9.5	-13.9	-27.2	-30.4	-12.6	0.0	-0.6

6

- 1 **Table 7. Changes in surface SOA concentrations due to a 50% reduction in**
- 2 **anthropogenic NO emissions.** Total SOA changes from each model are listed for global
- 3 average, the southeast U.S. and the Amazon.

		Concentration in Control run (ng/m³)	Standard deviation (ng/m³)	Concentration change in sensitivity run (ng/m³)	Percentage change
SE US [32°-40°N, 95°-77°W]	2-product	1638	248	-119	-7.3%
	VBS	2005	286	-127	-6.4%
	VBS_agHigh	4331	594	-518	-12.0%
Amazon [17°S-5°N, 77°-55°W]	2-product	3360	1383	-30	-0.9%
	VBS	3884	1197	-46	-1.2%
	VBS_agHigh	5390	1542	-153	-2.8%
Global average	2-product	358	40	-3.6	-1.0%
	VBS	393	37	-3.6	-0.9%
	VBS_agHigh	774	52	-43	-5.6%

4

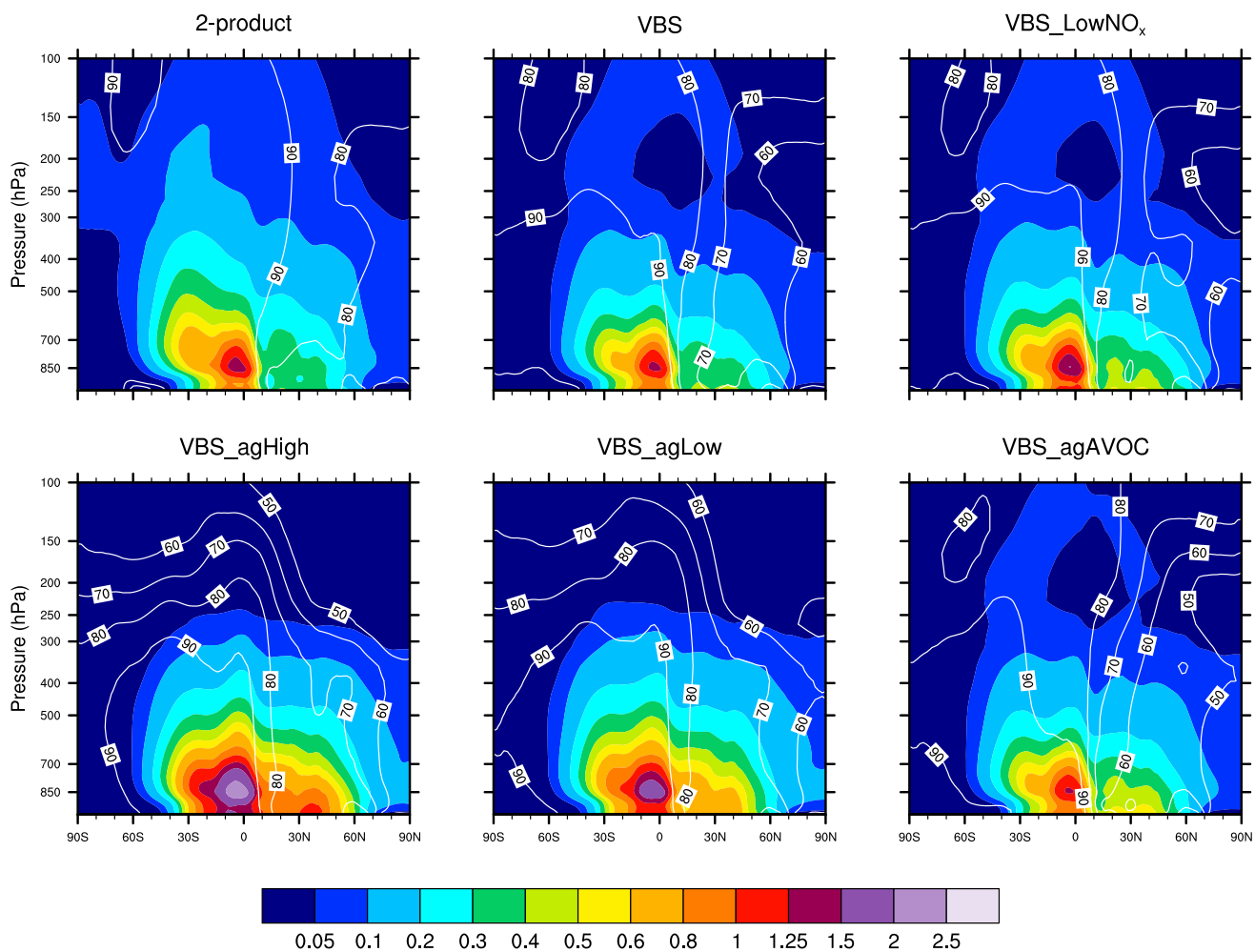


Figure 1. Annual mean zonally averaged SOA concentration ($\mu\text{g m}^{-3}$) (shown as colored shades) and the fraction of biogenic SOA (%) (shown as white contours) in CAM4-chem for different SOA treatments.

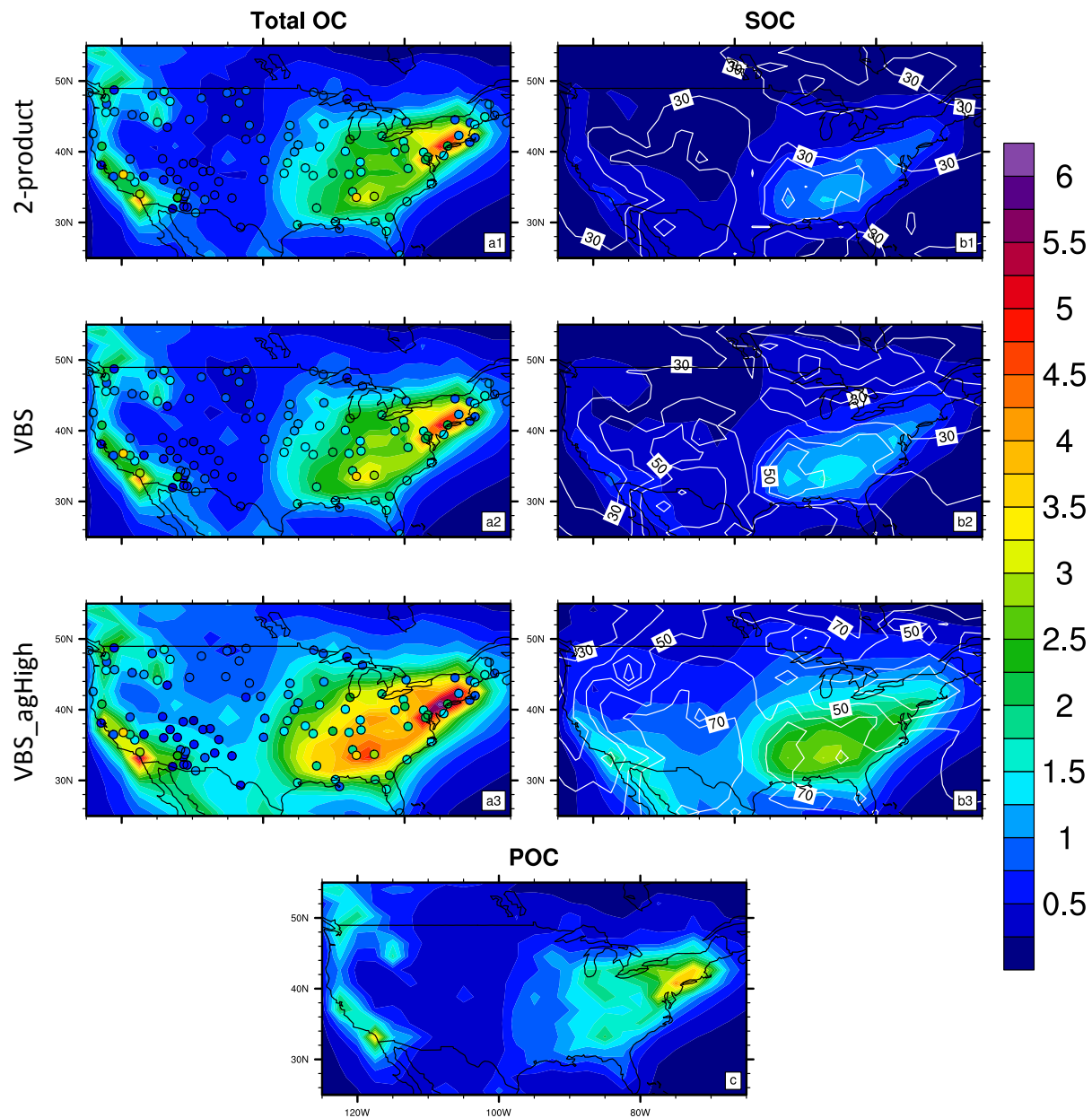


Figure 2. Annual mean surface concentrations (units: $\mu\text{g}[\text{C}] \text{ m}^{-3}$) of (a1)~(a3) total organic carbon (OC=POC+SOC), (b1~b3) secondary organic carbon (SOC) and (c) primary organic carbon (POC). The data is averaged from 2005 to 2009. In (a1)~(a3), scatters are IMPROVE observations and color shades are simulated total OC from the model 2-product, VBS and VBS_agHigh. In(b1)~(b3), white contours indicate the fraction of SOC in total OC (%), ranging from 30% to 70% with an interval of 10%. (c) shows simulated POC, which is identical in the 3 simulations.

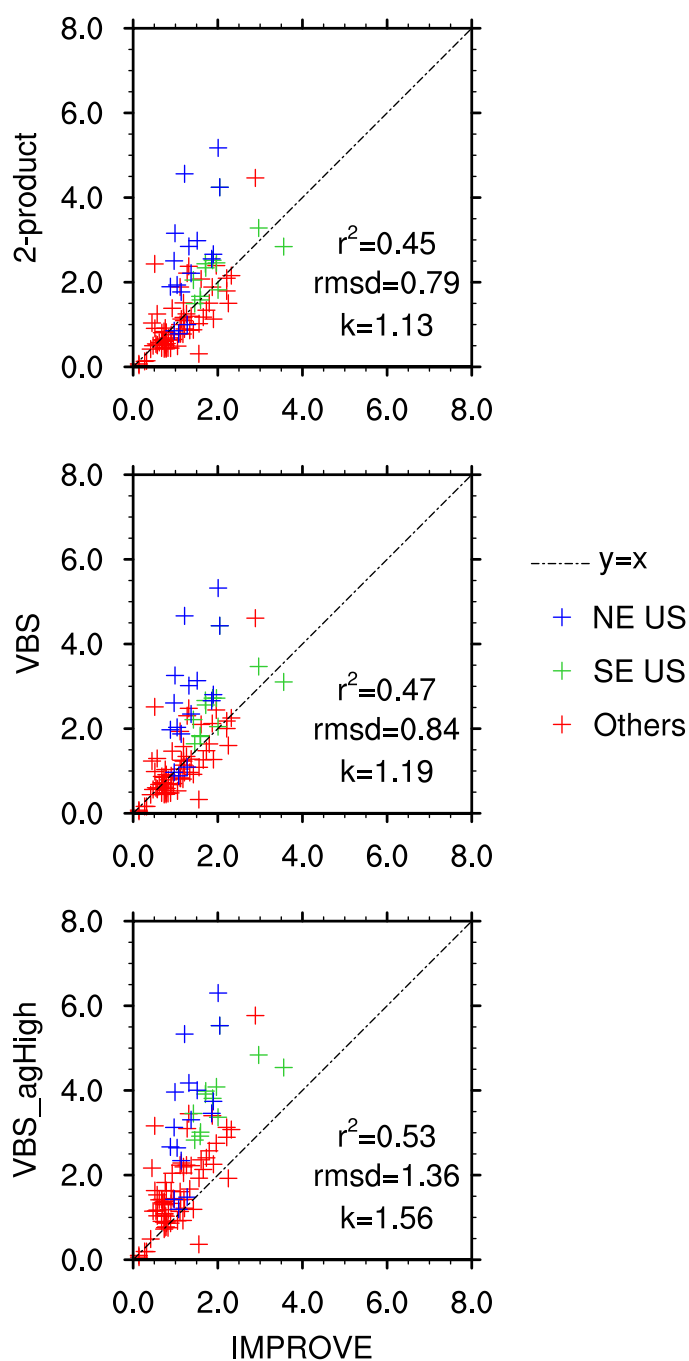


Figure 3. Comparison of averaged annual mean surface OC concentrations ($\mu\text{g}[\text{C}] \text{ m}^{-3}$) between IMPROVE measurements and the three simulations: 2-product, VBS and VBS_agHigh. Different colors indicate sites in different regions. In each subplot, the dash line is 1-to-1 line. The coefficients of determination (r^2), root-mean-square-difference (rmsd) and the model-to-observation slope (k) are included.

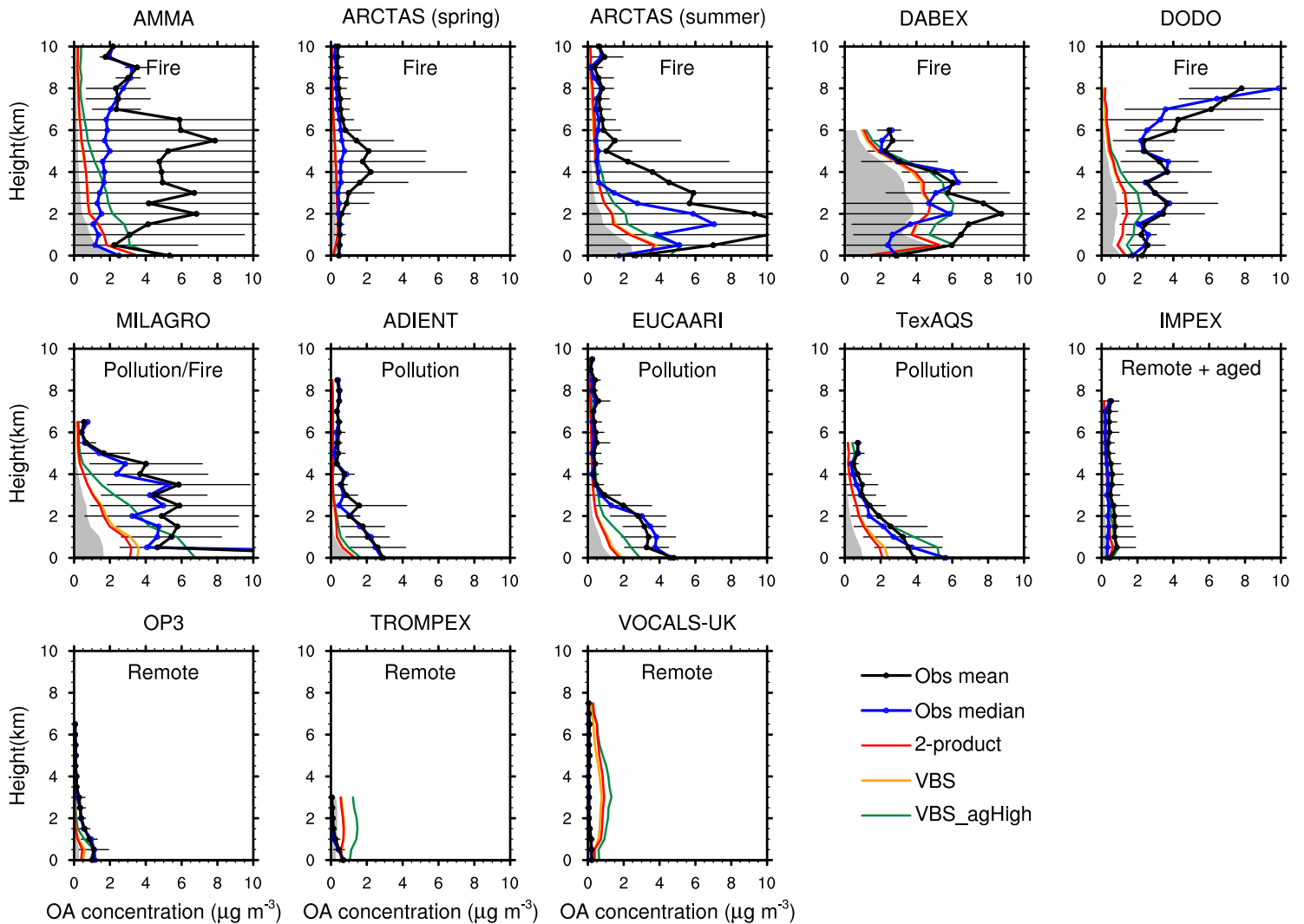


Figure 4. Comparison between observed vertical profile of OA concentration ($\mu\text{g m}^{-3}$) from 13 AMS field campaigns and the three model simulations: 2-product, VBS and VBS_agHigh. The campaign information is summarized in Heald et al. (2011) (Fig. 1 and Table 1 therein). The error bars are one standard deviation of the binned observations for each 0.5 km interval. The grey shades are simulated POA assuming a POA-to-POC ratio of 1.4. The model simulations are sampled for the corresponding months and locations for each campaign. The location and location type for each campaign is included in each subplot.

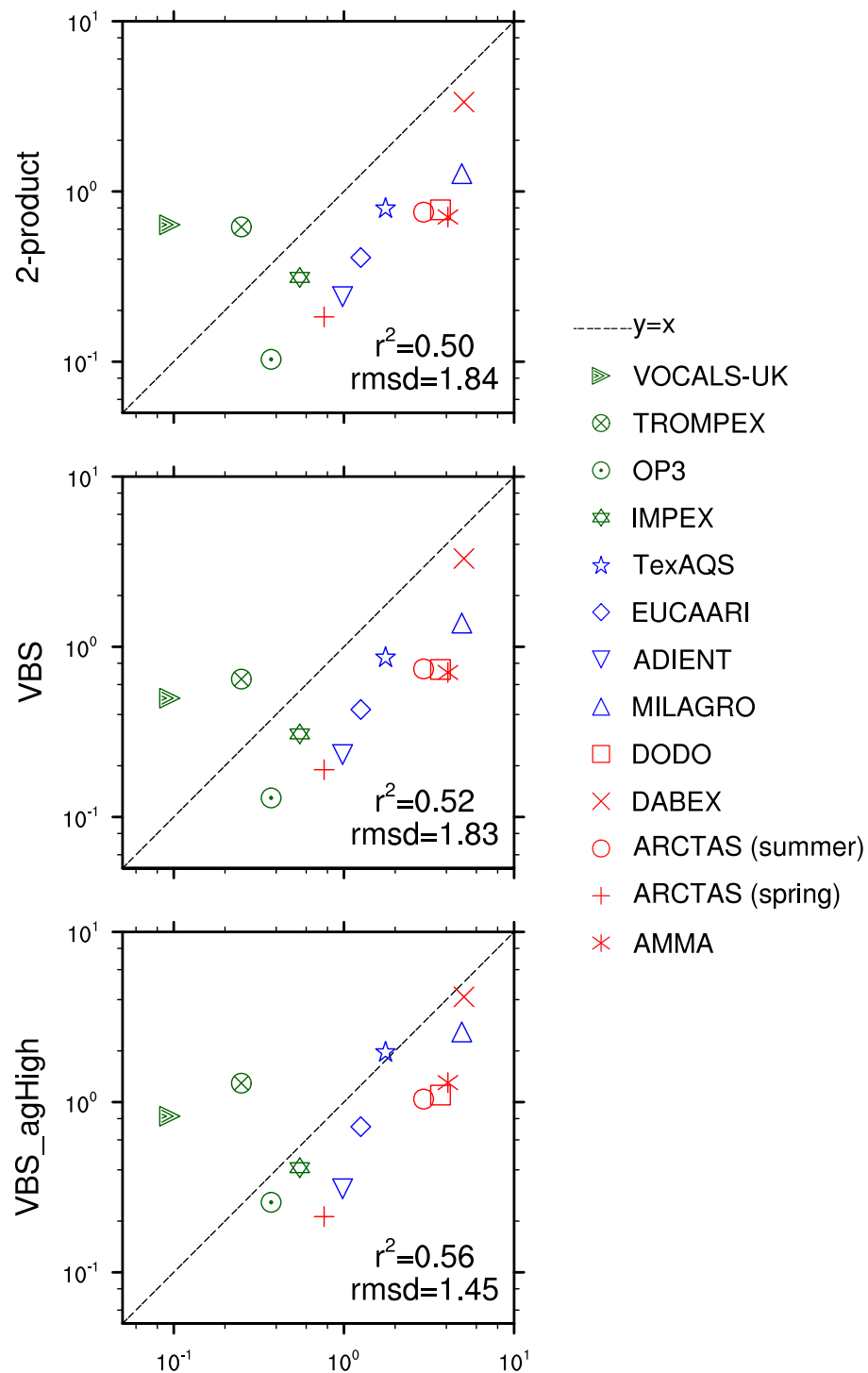


Figure 5. Comparison between averaged OA concentration ($\mu\text{g m}^{-3}$) from 13 AMS field campaigns and the 3 model simulations: 2-product, VBS and VBS_agHigh. The campaign information is summarized in Heald et al. (2011) (Fig. 1 and Table 1 therein). All data in each campaign are temporally, horizontally and vertically averaged to a single value, and compared to the model outputs averaged over the same period and location.

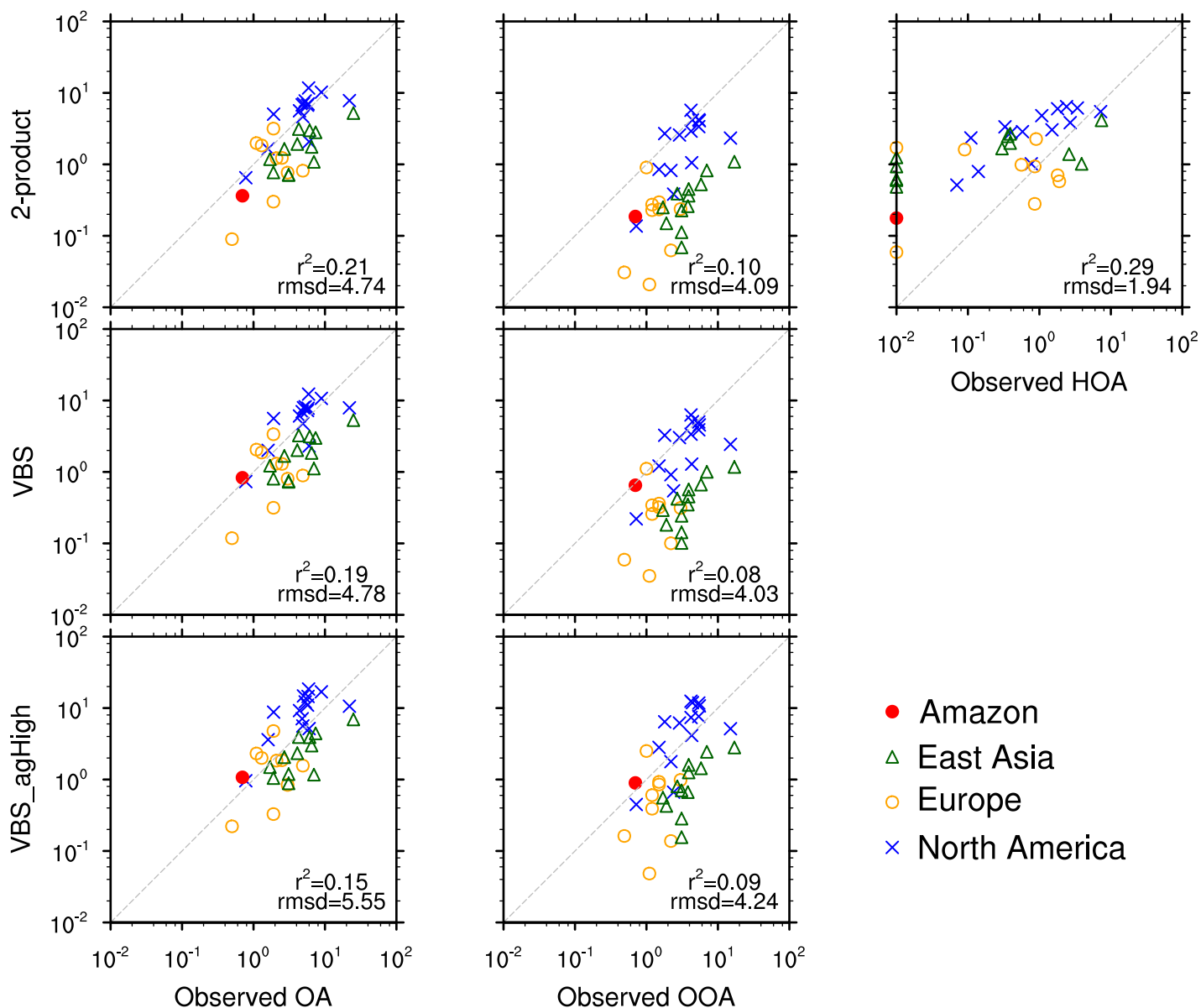


Figure 6. Comparison of surface AMS measurements (units: $\mu\text{g m}^{-3}$) and three simulations (first column: total OA; second column: SOA(OOA); third column: POA(HOA)). The coefficients of determination (r^2) and root-mean-square-difference (rmsd) are included in each subplot. The observed oxygenated OA (OOA) is a surrogate for SOA from all sources. The observed hydrocarbon-like OA (HOA) is a surrogate for POA from combustion and biomass burning. Simulated POA is identical in the three simulations. In POA-HOA comparison, data points with observed HOA smaller than $0.01 \mu\text{g m}^{-3}$ have been set to $0.01 \mu\text{g m}^{-3}$ to be shown in the plots.

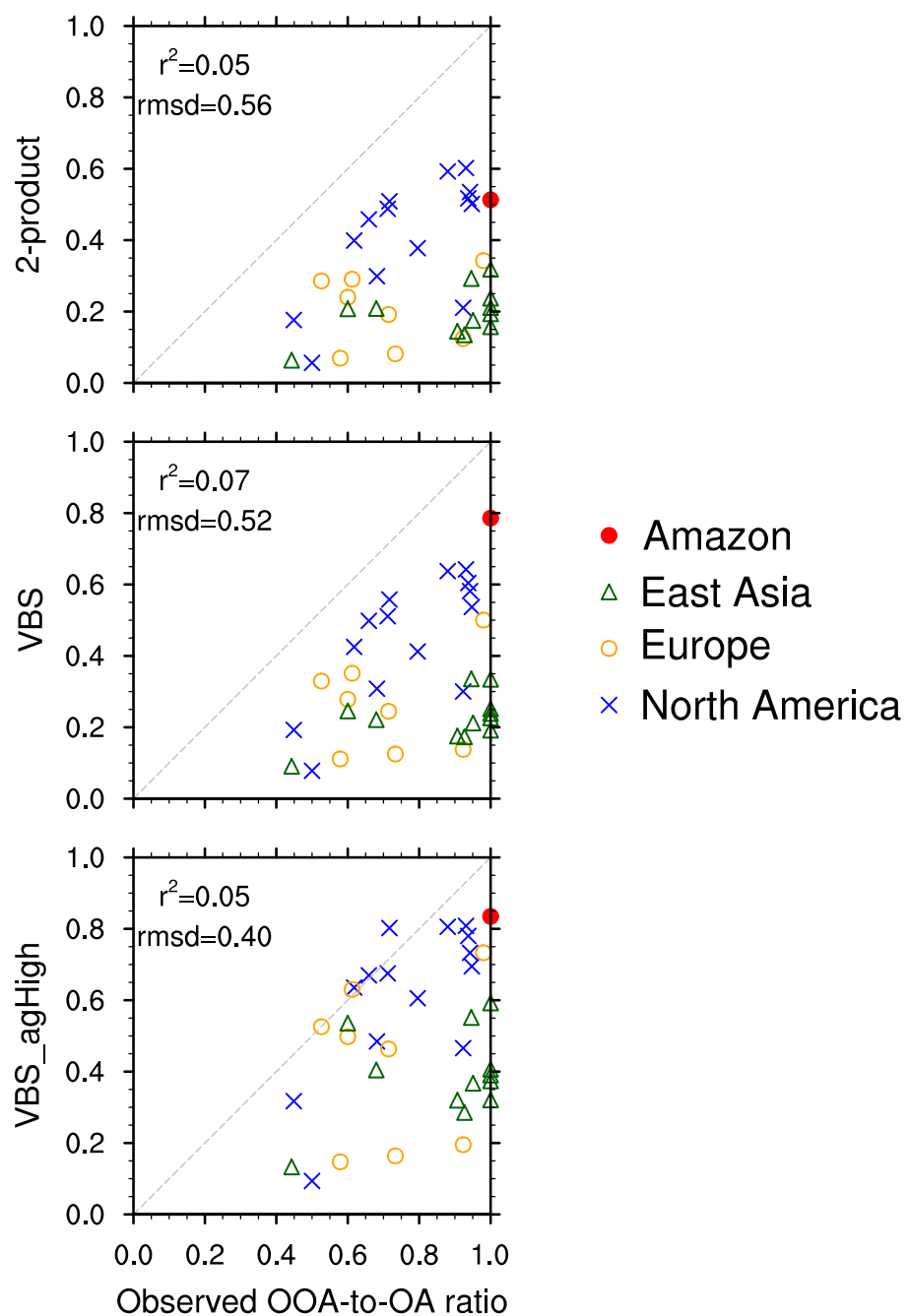


Figure 7. Comparison of observed OOA-to-OA ratio from surface AMS measurements and simulated SOA-to-OA ratio from the 2-product, VBS and VBS_agHigh schemes. The coefficients of determination (r^2) and root-mean-square-difference (rmsd) are included in each subplot.

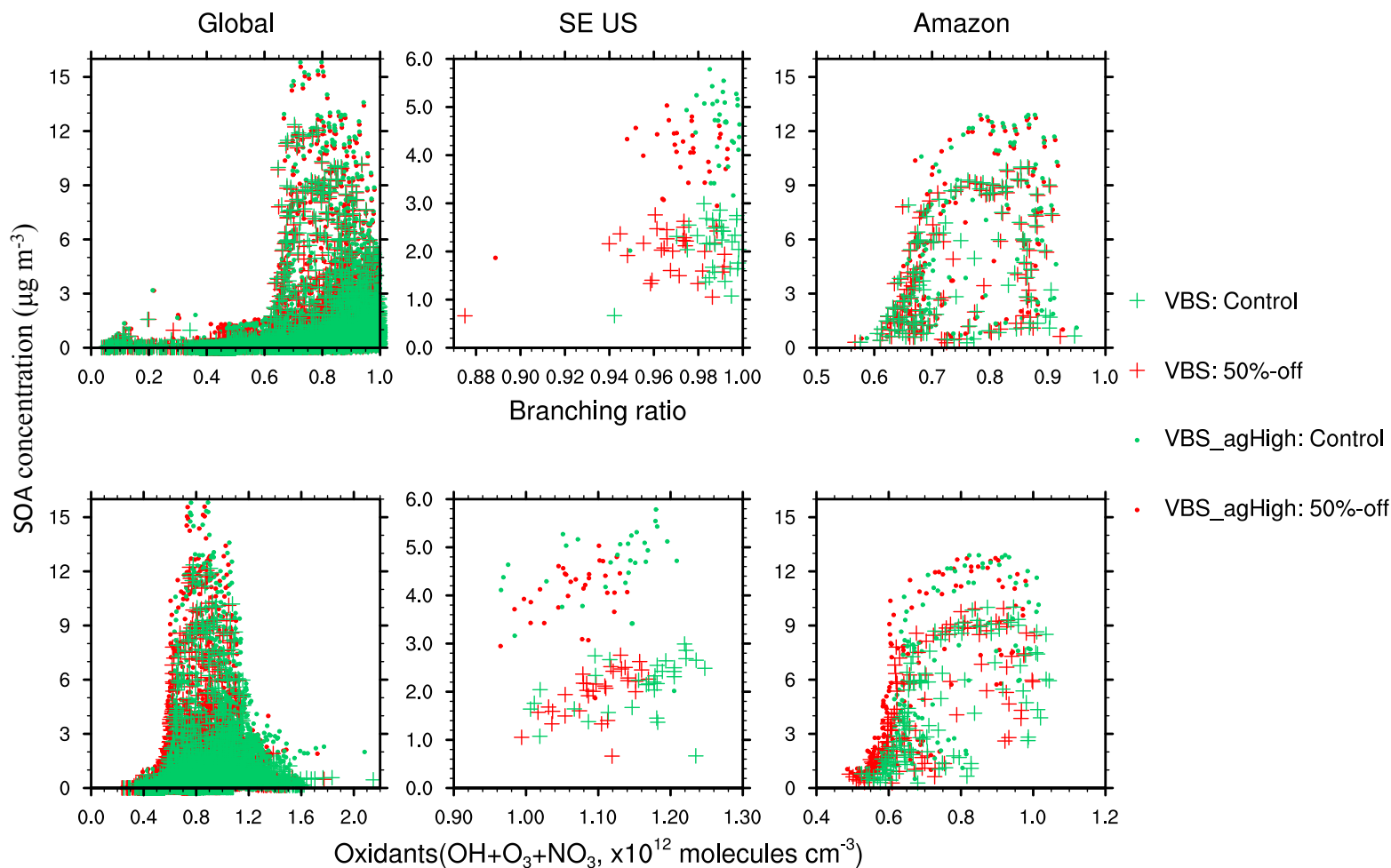


Figure 8. Dependence of annual mean surface SOA concentration ($\mu\text{g m}^{-3}$) on branching ratio and oxidants level at global scale, in the southeast US and the Amazon. The control runs and the sensitivity runs using VBS and VBS_agHigh schemes are shown. The 2-product results are similar to the VBS results (not shown). Data points over ocean are excluded. Note that the scales for the southeast US and the Amazon are different from the global subplots.

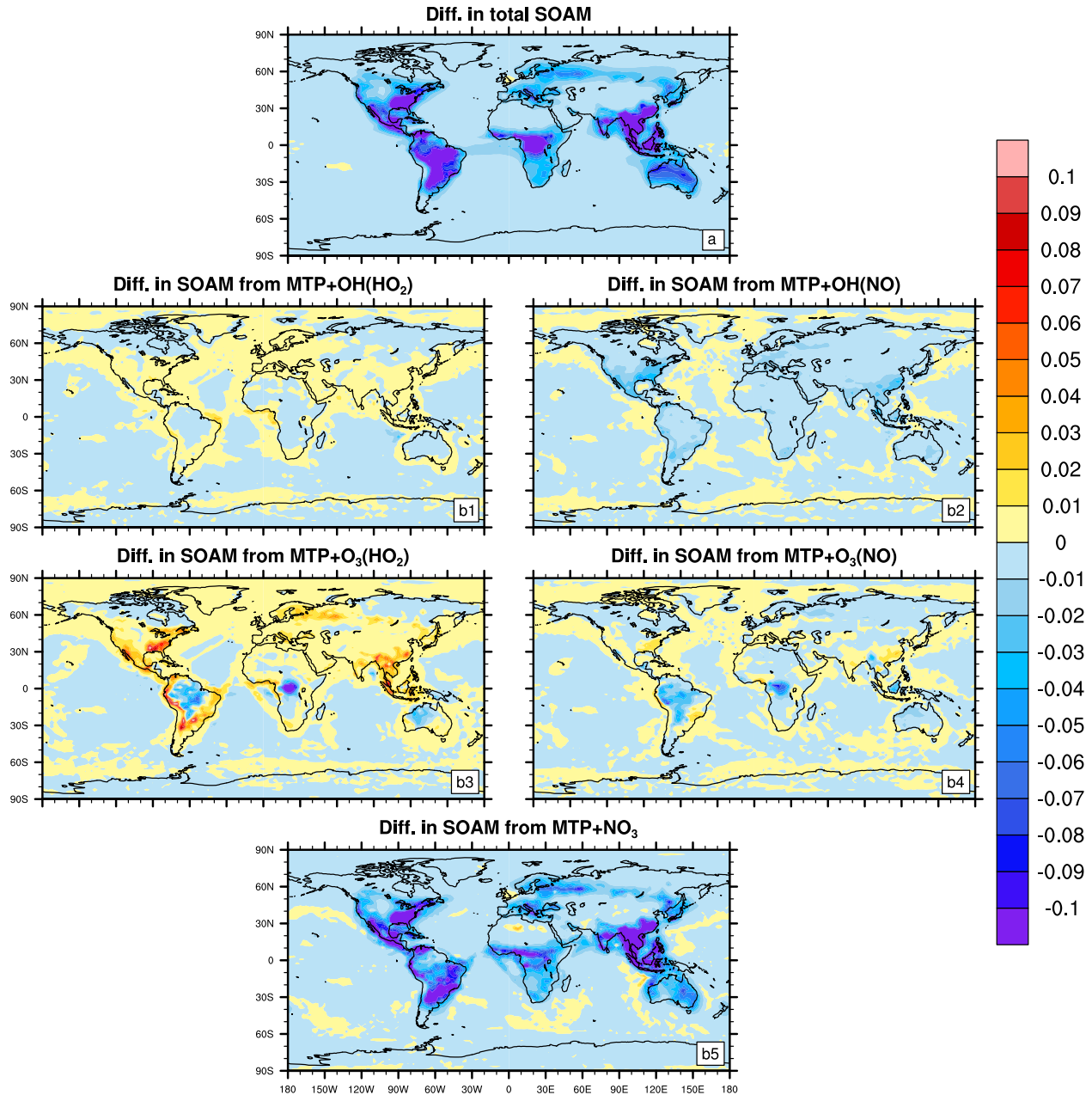


Figure 9. Changes in surface monoterpene SOA (SOAM) concentration ($\mu\text{g m}^{-3}$) in the sensitivity run with 50% reductions in anthropogenic NO emissions compared to the control run using VBS_agHigh scheme. The total SOAM change is shown in (a). The SOAM change in each formation branch is denoted as: (b1): MTP+OH(HO_2) (low- NO_x OH-photooxidation); (b2): MTP+OH(NO) (high- NO_x OH-photooxidation); (b3): MTP+ O_3 (HO_2) (low- NO_x ozonolysis); (b4): MTP+ O_3 (NO) (high- NO_x ozonolysis); (b5): MTP+ NO_3 (NO_3 -initiated oxidation).

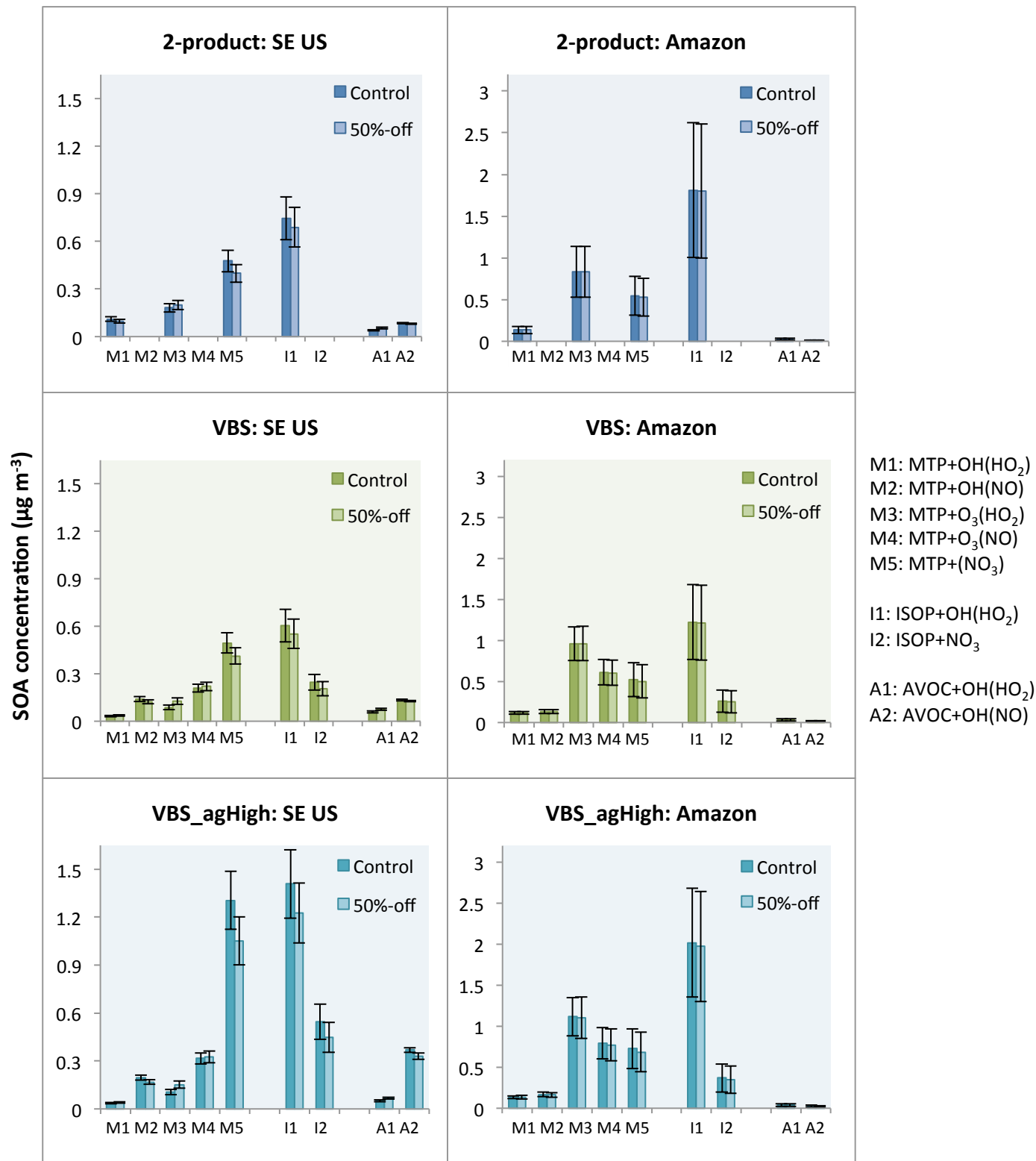


Figure 10. Annual mean surface SOA concentration ($\mu\text{g m}^{-3}$) in the control runs and the sensitivity runs (with 50% anthropogenic NO emission off) from different pathways, averaged over the southeast U.S. [32° - 40°N , 95° - 77°W] and the Amazon [17°S - 5°N , 77° - 55°W].